# We are IntechOpen,
# the world's leading publisher of
# Open Access books
# Built by scientists, for scientists

## 6,900
Open access books available

## 185,000
International authors and editors

## 200M
Downloads

## 154
Countries delivered to

Our authors are among the

## TOP 1%
most cited scientists

## 12.2%
Contributors from top 500 universities

**CLARIVATE ANALYTICS**
**BOOK CITATION INDEX**
**INDEXED**

**WEB OF SCIENCE**™

Selection of our books indexed in the Book Citation Index
in Web of Science™ Core Collection (BKCI)

# Interested in publishing with us?
# Contact book.department@intechopen.com

Numbers displayed above are based on latest data collected.
For more information visit www.intechopen.com

# Origin of Piezoelectricity on Langasite

Hitoshi Ohsato[1,2,3]
*[1]Hoseo University,*
*[2]Nagoya Institute of Technology,*
*[3]Nagoya Industrial Science Research Institute,*
*[1]Korea*
*[2,3]Japan*

## 1. Introduction

Piezoelectric materials produce polars in the crystal structure and charges on the surface of the crystal, when the crystals are stressed mechanically as shown in Figure 1(a). The surface charges leads to a voltage difference between the two surfaces of the crystal. On the contrary, when the crystals are applied with an electric field, they exhibit mechanical strain or distortion as shown in Figure 1(b).
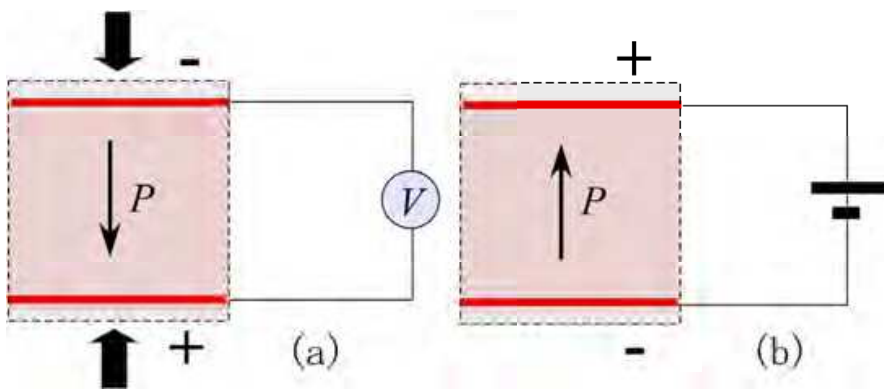


Fig. 1. The piezoelectric effects. (a) generated $V$ by an applied force. (b) compressed crystal by an applied voltage.
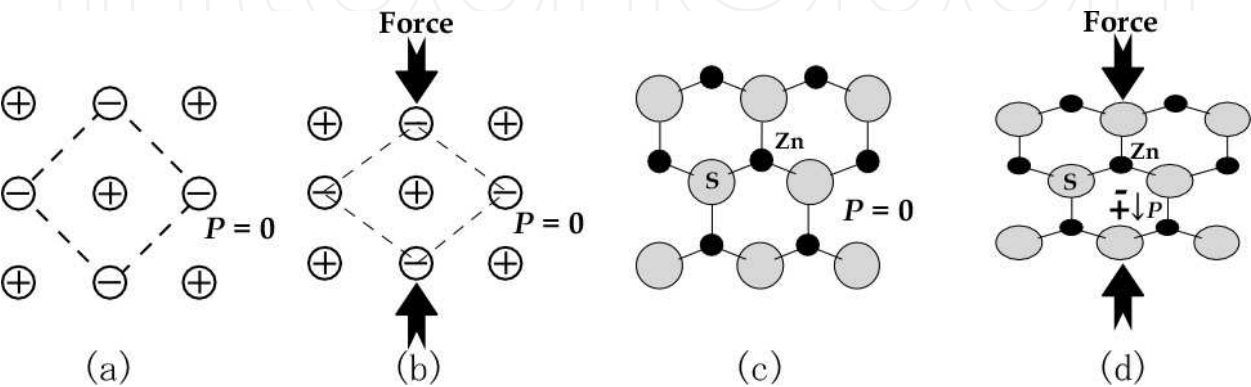


Fig. 2. (a) and (b) NaCl type crystal with $i$. (c) and (d) Hexagonal unit cell without $i$.

The crystal structure of piezoelectric materials should be no center of symmetry $i$ that is inversion symmetry. Figure 2(a) and 2(c) shows the crystal structure with $i$ and without $i$, respectively. The first one is NaCl structure with $i$, in which the centers of mass of positive charges and negative charges are in the same position. This case, a net dipole moment $P$ does not appear in the crystal structure. Under mechanical stress, also the $P$ moment does not appear, though the polarity appears under the electric field. The second one is ZnS zincblende without $i$, in which the centers of mass of positive and negative charges are in the same position as shown in Figure 2(c). However, under stress as shown in Figure 2(d), the centers of mass of positive charges and negative charges are in different positions. In this case, a net dipole moment $P$ appears in the crystal structure, which is piezoelectricity.

These piezoelectric materials without $i$ are included in point groups (except $O = 432$) of 2nd to 7th columns as shown in Table 1. Here, the 1st column is Laue group with $i$, and 3rd to 6th for optical activity, 5th to 7th for pyroelectricity, and 4th and 5th for enantiomorphism. Ferroelectric materials are ones with spontaneous polarization in pyroelectricity 5th to 7th. All ferroelectric materials show piezoelectricity, but the reverse is not true, that is, not all piezoelectric materials show ferroelectricity.

Piezoelectric materials such as quartz, topaz, Rochelle salt, and tourmaline and so on were discovered in 1880 by the Curie brothers. Quartz single crystal is one of the most useful piezoelectric materials. The point group is 32 of the 4th group in Table 1 which is none polar piezoelectric material. As the electromechanical coupling factor is small but temperature coefficient of resonant frequency ($TCf$) is near zero ppm/°C, quartz has been used for bulk transducer and SAW devices. Artificial quartz single crystals fabricated by hydrothermal synthesis have been used for these devices because natural single crystals are deteriorated by Brazil-type twin weaken the piezoelectricity due to co-existence of right and left hand crystals (Figure 3(a)) in a crystal as shown. The twin brings high symmetry producing mirror symmetry by screw axes $3_1$ and $3_2$ as shown in Figure 3(b). Lithium Niobate $LiNbO_3$ (LN) and Lithium Tantalate $LiTaO_3$ (LT) single crystals are used widely for SAW filter, resonator et al., which are treated poling for adjusting the polar directions because of the ferroelectrocity based on the point group $3m$ and space group $R3c$.

Lead-zirconate-titanate $Pb(Zr,Ti)O_3$ (PZT) ceramics located on the morphtropic phase boundary (MPB) co-existing trigonal and tetragonal phases has been used for bulk piezoelectricity transducer, resonator, and SAW filter, as it shows excellent piezoelectricity that has a huge electromechanical coupling factor. Though the PZT is standing at a critical moment because of toxins for health, still it is being used for industrial applications. As PZT ceramics composed by tetragonal and trigonal crystals, point group $4mm$ (space group: $P4mm$) and $3m$ ($R3m$), respectively, belonging No.7th group in Table 1, they are ferroelectrics having polar. So, poling treatments are useful for improving the piezoelectricity. The properties of the binary PZT compound between $PbZrO_3$ and $PbTiO_3$ are improved more adding $Pb(Mg_{1/3}Nb_{2/3})O_3$. The three components perovskite compounds are used IF SAW filter on 10 to more MHz region. Furthermore, the properties of these perovskite compounds are improved by applying single crystals by Hosono & Yamashita (2004) as shown in Figure 4.

Recently, Pb-free piezoelectric materials have been researched because of the toxin of Pb for health. It was applied as restriction of hazardous substances (RoHs) from 1 July 2006 based on directive 2001/95/EC of the European Parliament and of the Council of 27 January 2003,

| | 1 | 2 | 3 | 4 | 5 | 6 | 7 | Crystal system |
|---|---|---|---|---|---|---|---|---|
| 1 | $C_i = \bar{1}$ | | | | $C_1 = 1$ | | | Triclinic |
| 2 | $C_{2h} = 2/m$ | | | | $C_2 = 2$ | $C_s = m$ | | Monoclini |
| 3 | $D_{2h} = mmm$ | | | $D_2 = 222$ | | $C_{2v} = mm2$ | | Orthorhombic |
| 4 | $C_{4h} = 4/m$ | | $S_4 = \bar{4}$ | | $C_4 = 4$ | | | Tetragonal |
| 5 | $D_{4h} = 4/mm$ | | $D_{2d} = \bar{4}2m$ | $D_4 = 422$ | | | $C_{4v} = 4mm$ | |
| 6 | $C_{3i} = \bar{3}$ | | | | $C_3 = 3$ | | | Hexagonal |
| 7 | $D_{3d} = \bar{3}m$ | | | $D_3 = 32$ | | | $C_{3v} = 3m$ | |
| 8 | $C_{6h} = 6/m$ | $C_{3h} = \bar{6}$ | | | $C_6 = 6$ | | | |
| 9 | $D_{6h} = 6/mm$ | $D_{3h} = \bar{6}m2$ | | $D_6 = 622$ | | | | |
| 10 | $T_h = m3$ | | | $T = 23$ | | | | Cubic |
| 11 | $O_h = m3m$ | $T_d = \bar{4}3m$ | | $O = 432$ | | | | |
| | Laue group | | | Enantiomorphism | | | | |
| | | | | | Pyroelectricity | | | |
| | | | Optical activity | | | | | |
| | Piezoelectricity (except 432) | | | | | | | |

Table 1. Point groups and properties.



*Natural crstal with Brazil-type twin. m-symmetry is added.*

(a)

*Left-hand and Right hand crystals Enantiomorphism*
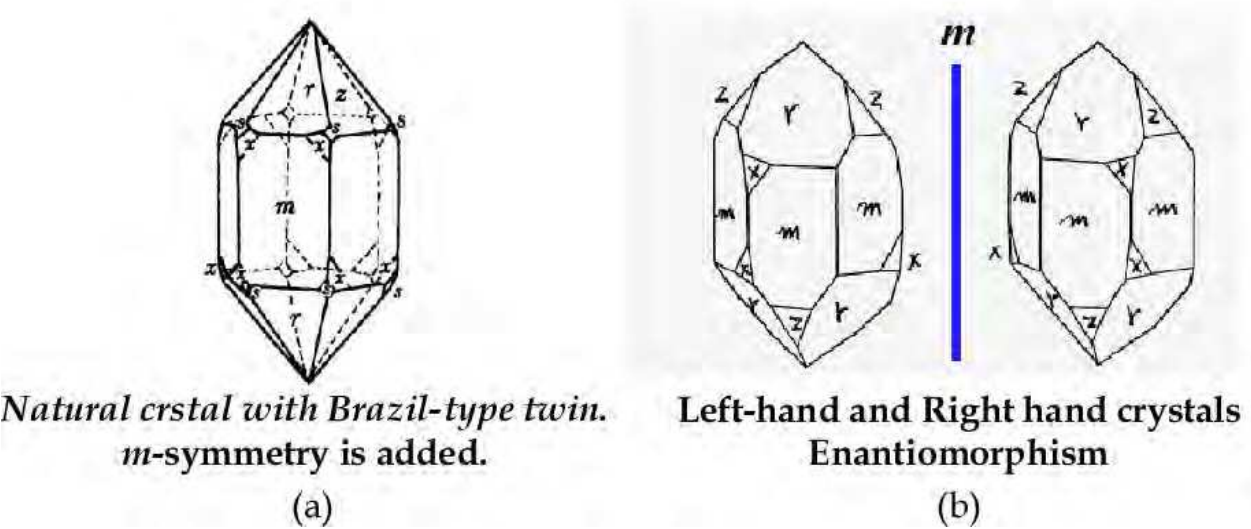
(b)

Fig. 3. Natural quartz crystal (a) including Brazil-type twin of right and left hand crystals (b). $m$: mirror plane.

that new electrical and electronic equipment put on the market does not contain lead, mercury, cadmium, hexavalent chromium, polybrominated biphenyls (PBB) or polybrominated diphenyl ethers (PBDE) as appeared in Article 4 of the directive [web site 1]. Lead in electronic ceramic parts (e.g. piezoelectric devices) has been excluded from the RoHs directive as appeared in the Annex of the directive.
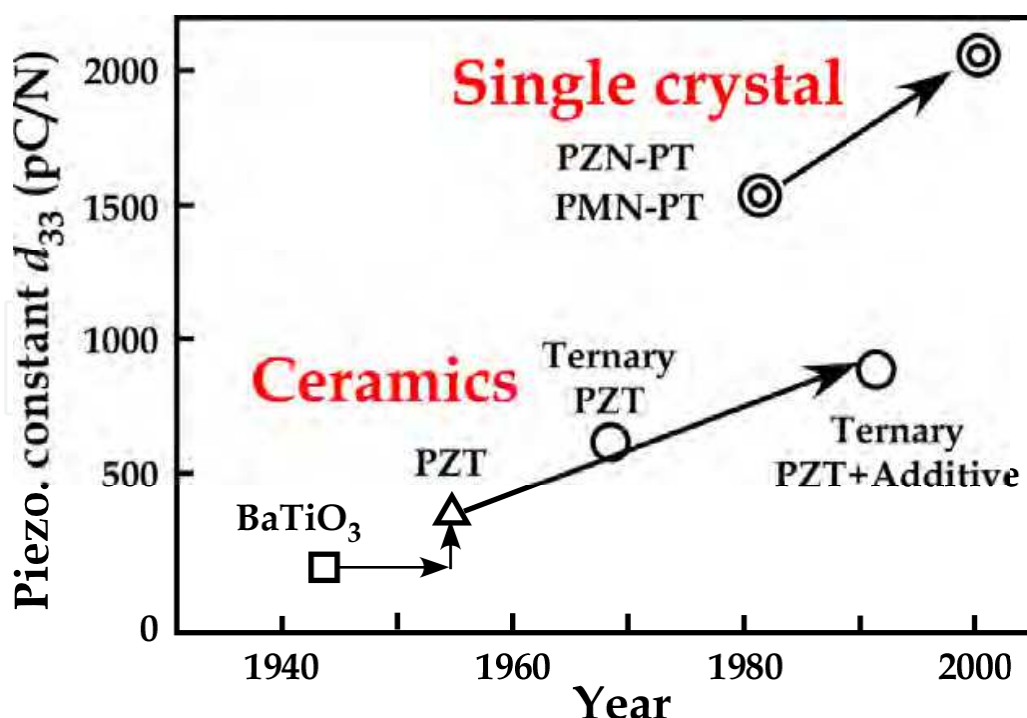
Fig. 4. Trend of piezoelectric materilas.

There are candidate materials for the Pb-free piezoelectric materials such as niobate based ceramics group, tungsten-bronze group, and perovskite relative materials. In the author's laboratory, $KNO_3$ being basically hard sintering materials was successfully formed as high density ceramics co-doping of $La_2O_3$ and $Fe_2O_3$ by Kakimoto et al. (2004), and Guo et al. (2004) found $[Li_{0.06}(Na_{0.5}K_{0.5})_{0.94}]NbO_3$ ceramics with excellent piezoelectric constant $d_{33}$ values reach 235 pC/N on the MPB. Saito (2004) also fabricated highly orientated $(Na_{0.5}K_{0.5})NbO_3$-$LiTaO_3$ (NKN-LT) ceramics by template method. With the $d_{33}$ values reach 400 pC/N. Langasite $La_3Ga_5SiO_{14}$ (LGS) group crystals are also Pb-free piezoelectric material, which are being reviewed just in this chapter, presented by Mill et al. (1982) and Kaminskii et al., (1983).

The target of in this chapter is to state mechanism of piezoelectricity on Langasite. So, some mechanisms of piezoelectricity should be presented here. Figure 5 shows mechanism of piezoelectricity in the case of BeO. Figure 5(a) is crystal structure of BeO in the absence of an applied force, here, +: Be, -:O. Under an applied force, the center of mass for positive and negative ions are different positions producing a net dipole moment $P$ which generate negative and negative charges on the surfaces as shown in Figure 5(b). In the case of quartz $SiO_2$ which is the most important piezoelectric material, the structure is also constructed by six membered $SiO_4$ rings. The mechanism of piezoelectricity is similar with BeO, which is produced by the deformation of the six membered ring. Perovskite structures which are very important crystal structure for electro materials show very great piezoelectricity. The structure has some polymorphs such as cubic, tetragonal, orthorhombic and hexagonal. Cubic structure has center of symmetry $i$, and transform to tetragonal without $i$ at curie temperature about 120 °C for $BaTiO_3$.

In this chapter, LGS, $Pr_3Ga_5SiO_{14}$ (PGS) and $Nd_3Ga_5SiO_{14}$ (NGS) single crystals grown by Czochralski method were analysed the crystal structure by X-ray single crystal diffraction

(XRSD) and clarified the differences of crystal structure. The mechanism of the piezoelectricity was clarified based on the crystal structure, which was confirmed by the deformation of the crystal structure under high pressure. Also relationships between the crystal structure and the properties are discussed, and it was also clarified that LGS has higher piezoelectric properties than NGS.
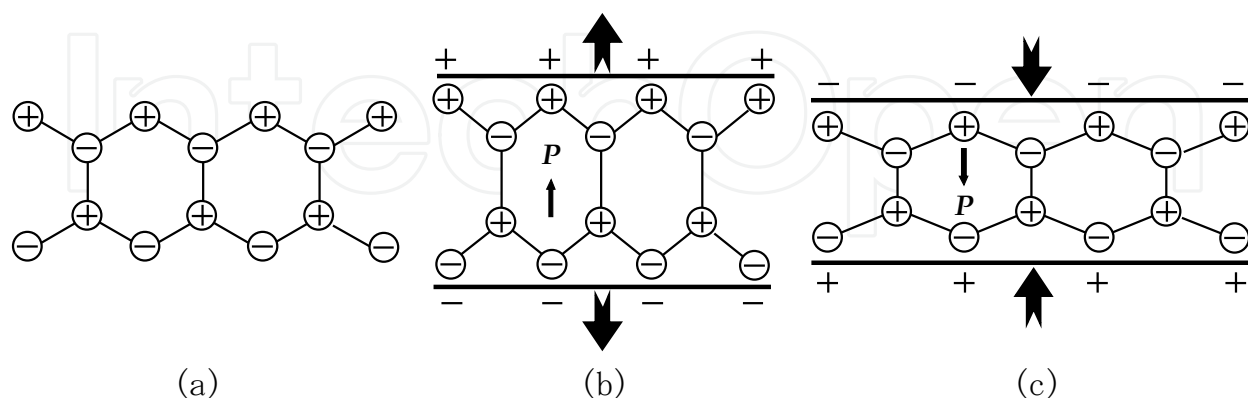


Fig. 5. Mechanism of piezoelectricity of BeO. +: Be ion, -: O ion.

## 2. Crystal growth of langasite

Langasite group single crystals have been grown by many growing methods such as Czochralski (Cz) technique, Bridgeman method, floating zone (FZ) method, micro-pulling down (μ-PD) technique, as these crystals grow easily because of a low melting point around 1470 °C being able to use stably Pt-crucible, no phase transition and congruent melting. The most useful method is Cz-method which is pulling up a single crystal using the seed crystal from melts in a crucible heated (Figure 6(a)-(c)). Bridgeman method is easy, which is grown in a crucible with gradient temperature spontaneously nucleating in the bottom of the crucible. FZ-method has a melting and crystallizing zone between seed crystal and sintered ceramic rod with same composition as grown crystal, which is grown without contamination because of no crucible. The viscosity of langasite crystals is considered suitable for FZ-method, because the ratio between oxygen ions and cations in tetrahedra $C$ and $D$-site in the crystal structure $A_3BC_3D_2O_{14}$ is 2.8, locating near one dimensional or ring framework with 3. μ-PD method is special which grows long size thin single crystal with around 1mm $\phi$ by few cm meters to over one meter (Figure 6(d)). A single crystal grows during pulling down from the bottom small hole of a container made by a heater such as Pt. LGS, PGS and NGS single crystals as shown used in this chapter were grown by a conventional radiation frequency (RF)-heating Cz-method with output power 60kW by Sato et. al. (1998). Starting melts formed from single-phase powder of langasite sintered 1300 °C using high purity 99.99 % low materials were applied a height of 40 mm in platinum and iridium crucible with 50 mm in diameter and 50 mm in height. The growth atmosphere was a mixture of Ar and 1 vol % of $O_2$ gases in order to avoid the evaporation of gallium oxide from the melt during growth. The heating of melts was performed by Pt-crucible itself by induction heating. The crucible was isolated by $ZrO_2$ granules. Before seeding, the melts was clarified during 1 h at least. The pulling velocity and the crystal rotation rates were 1.0-1.5 mm/h and 10 rpm, respectively. The seeds were used a small <001> oriented LGS single crystal rods. Growing crystal was kept the temperature by a passive double after-heating system made of alumina ceramics.
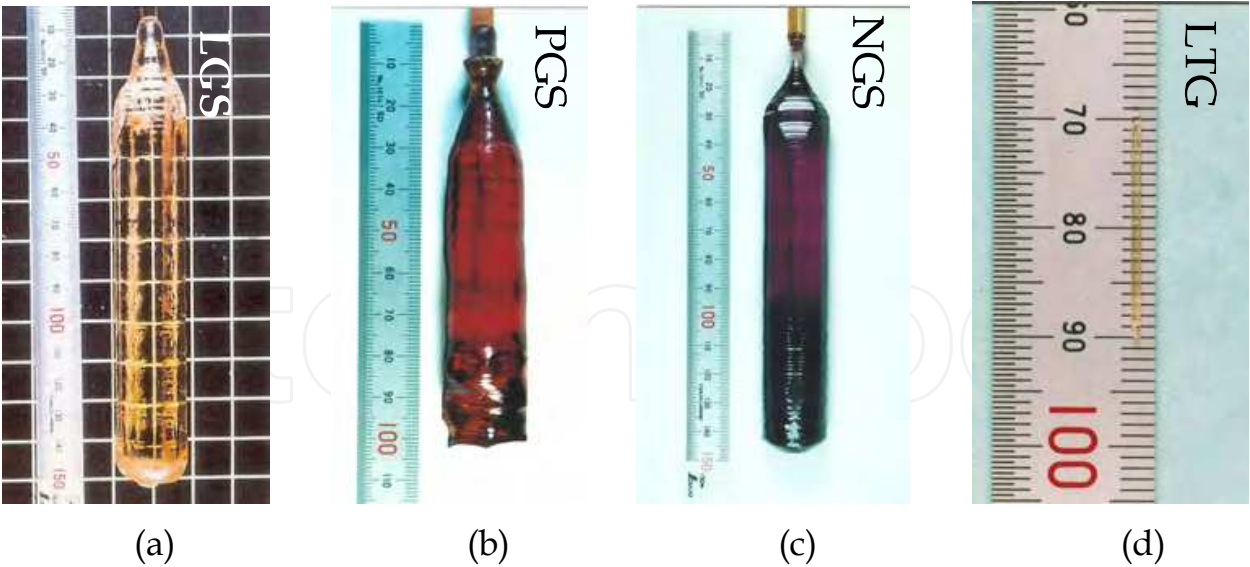
Fig. 6. Single crystals of Langasite (a)-(c) and (d) grown by Cz-method, and by μ-PD technique, respectivery.

Defect-free LGS, PGS and NGS single crystals with constant diameter of 22 mm and lengths up to 145 mm were grown as shown in Figure 6(a), (b) and (c), respectively (Sato et al., 1998). These ingot diameters were high constancy over the whole length. The optimum pulling rates are not exceeding 1.5 mm/h for inclusion-free perfect single crystals, and a higher temperature gradient at the growing interface controls the growth preventing a distinct facet enlargement and asymmetrical growth leading to spiral morphology.
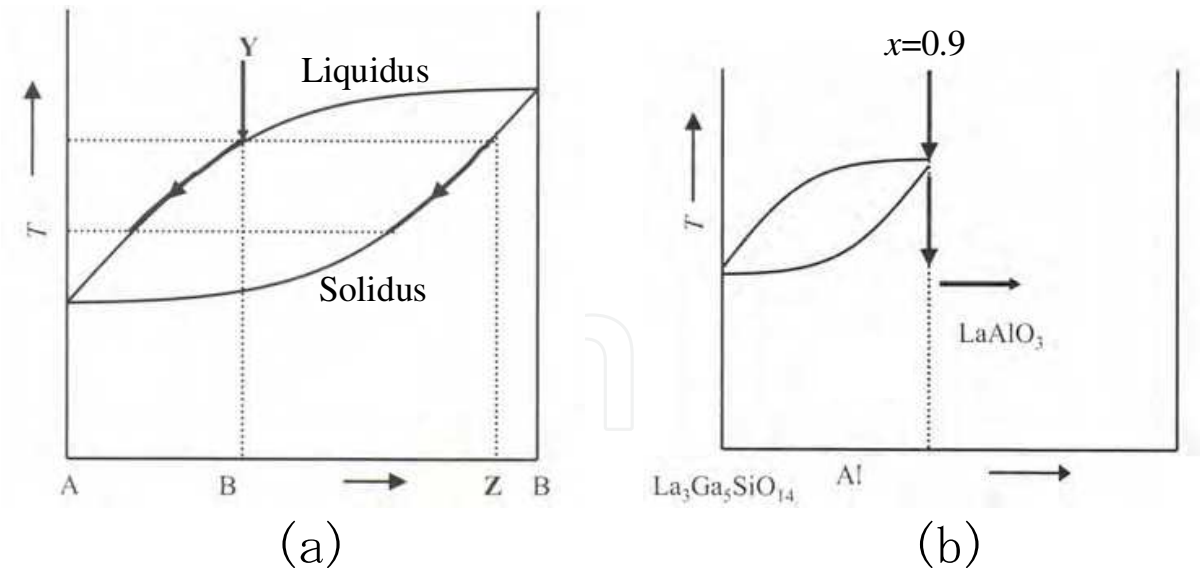


Fig. 7. Crystal growth from quasi-congruent melt. (a) Crystal growth of solid solutions: composition of precipitaed should be changed gradually. (b) Formatin of quasi-congruent melt at $x = 0.9$ due to precipitated secondary phase LaAlO$_3$.

LGS compounds with congruent melting are grown easily because of same composition of growth crystals and liquid. In the case of solid solutions, composition of precipitated crystal gradually changes during crystal growth as shown in Figure 7(a). Takeda & Tsurumi (2011)

presented crystal growth with homogeneous composition from quasi-congruent melt (Takeda, 1998, Kumatoriya et al., 2001). In the case of Al-substituted $La_3Ga_{5-x}Al_xSiO_{14}$ (LGAS$x$), as the limitation of the solid solutions is located at $x = 0.9$ as shown in Figure 7(b), endmember of the solid solutions makes congruent melt. At $x = 0.9$ composition, good quality single crystals of LGAS0.9 are grown as named quasi congruent melt growth.

|  | NGS | PGS | LGS |
|---|---|---|---|
| Composition | $Nd_3Ga_5SiO_{14}$ | $Pr_3Ga_5SiO_{14}$ | $LaGa_5SiO_{14}$ |
| Formula weight | 1033.401 | 1023.415 | 1017.409 |
| Crystal system | Trignal | Trignal | Trignal |
| Space group | $P321$ | $P321$ | $P321$ |
| Point group | 32 | 32 | 32 |
| Lattice parameter $a$ (Å) | 8.0674(5) | 8.0944(5) | 8.1674(4) |
| $c$ (Å) | 5.0636(9) | 5.0724(9) | 5.0964(8) |
| Unit cell volume (Å$^3$) | 285.40(5) | 287.81(6) | 294.41(5) |
| Formula number $Z$ | 1 | 1 | 1 |
| Calculated density $D_x$ (g/cm$^3$) | 6.0127 | 5.9047 | 5.7384 |
| Linear absorption coefficient $\mu$ (cm$^{-1}$) | 258.603 | 247.274 | 228.496 |
| $R$ | 0.0320 | 0.0292 | 0.0346 |
| $Rw$ | 0.0293 | 0.0264 | 0.0317 |
| $GOF$ | 1.2132 | 1.3497 | 1.2169 |

Table 2. Crystallographic data and reliability factors for crystal structure analysis of NGS, PGS and LGS.

## 3. Crystal structure of langasite

Langasite crystal structure was analyzed originally by Mill et al. (1982). The crystal structure is isostructural to $Ca_3Ga_2Ge_4O_{14}$ presented by Belokoneva et al. (1980). The crystal system is trigonal, point group 32, space group $P321$ (No.150), lattice constants approximately $a = 8.1$, $c = 5.1$ Å, $Z = 1$, which is similar as quartz $SiO_2$. We determined the three langasite-group LGS, PGS and NGS crystals using the initial atomic parameters presented by Mill et al. (1982). Table 2 shows the crystallographic data and experimental conditions for X-ray single crystal diffraction (XRSD) analysis. Sphere single crystals around 0.04 mm diameter grounded a cut single crystal were used for the single-crystal structure analysis performed by a four-circle diffractometer with graphite monochromer. After X-ray intensity data collected with MoK$\alpha$ radiation were corrected based on Lorentz and polarization ($Lp$) correction and absorption, the refinements of the crystal structure were performed by full-matrix least-squares program RADY (Sasaki, 1982). The site occupancy of $D$-site Ga:Si was obtained from multiplicity $g$ determined by the linear constrain as follows:

$$g(Ga) = cal. \tag{1}$$

$$g(Si) = 1/3 - g(Ga). \tag{2}$$

On the procedure of crystal structure analyzing, a scale factor, coordinates of each atoms, and anisotropic temperature factors were refined, and at final step of refinement, anisotropic extinction corrections were performed.

Table 3(a), 3(b), and 3(c) show atomic coordinates of LGS, PGS and NGS, respectively (Iwataki, 2002, Master thesis). The equivalent isotropic temperature factors ($B$eq.) were calculated using anisotropic temperature factors by following equation:

$$B_{eq.} = 1/3 \, \Sigma_i \, \Sigma_j \, B_{ij} \, a^*_i \, a^*_j \, a_i. \, a_j. \tag{3}$$

The $B_{eq.}$ values are reasonable as around 0.7 for cations and 1.5 for oxygen ions. And site occupancy ratios of Ga and Si ions in $D$-site are almost 1:1. The final reliability factors: $R$ and $R_w$ values are fine around 0.03.

The crystal structure figures projected from [001] and [120] are shown in Figure 8(a) and 8(b), respectively. The structure represented by the structural formula, $A_3BC_3D_2O_{14}$, is constructed four sites: $A$-, $B$-, $C$-, and $D$-site projected from two ways as shown in Figure 8. $A$-site is decahedron with eight coordination number (*c.n.*) named as twisted Thomson cube, $B$-site octahedron with six *c.n.*, and $C$- and $D$-sites tetrahedra with four *c.n.* as shown in Figure 8(c). The size of $D$-site is slightly smaller than that of $C$-site. Rare earth La$^{3+}$, Pr$^{3+}$ and Nd$^{3+}$ occupy the $A$-site, Ga$^{3+}$ occupies the $B$, $C$ and half of the $D$-sites, and Si$^{4+}$ half of the $D$-sites, respectively. This structure is constructed by framework layer structure: $B$-$C$-$D$-$C$-$D$-$C$ six-membered rings around $A$-site as shown in Figure 8(a) projected from [100]. Tetrahedra $C$- and $D$-site, and decahedra, octahedra and open-space form layer structure as shown in Figure 8(b). Large cation sites $A$- and $B$-sites, and open-spaces makes one layer. The open-space plays important role for piezoelectric properties as described in section 5.

(a) Atomic parameter of LGS

| atom | site | occupancy | $x$ | $y$ | $z$ | $B_{eq.}$ (Å$^2$) |
|------|------|-----------|-----|-----|-----|-------------------|
| La | 3*e* | 1 | 0.41865(3) | 0 | 0 | 0.625(3) |
| Ga1 | 1*a* | 1 | 0 | 0 | 0 | 0.844(8) |
| Ga2 | 3*f* | 1 | 0.76517(6) | 0 | 1/2 | 0.660(7) |
| Ga3<br>Si | 2*d* | 0.507(3)<br>0.493 | 1/3 | 2/3 | 0.5324(2) | 0.557(8) |
| O1 | 2*d* | 1 | 1/3 | 2/3 | 0.198(1) | 1.16(5) |
| O2 | 6*g* | 1 | 0.4660(4) | 0.3123(4) | 0.3186(6) | 1.41(7) |
| O3 | 6*g* | 1 | 0.2208(4) | 0.0811(4) | 0.7629(5) | 1.56(8) |

(b) Atomic parameter of PGS

| atom | site | occupancy | $x$ | $y$ | $z$ | $B_{eq.}$ (Å$^2$) |
|------|------|-----------|-----|-----|-----|-------------------|
| Pr | 3*e* | 1 | 0.41787(3) | 0 | 0 | 0.639(2) |
| Ga1 | 1*a* | 1 | 0 | 0 | 0 | 0.762(7) |
| Ga2 | 3*f* | 1 | 0.76473(5) | 0 | 1/2 | 0.656(6) |
| Ga3<br>Si | 2*d* | 0.498(3)<br>0.502 | 1/3 | 2/3 | 0.5346(2) | 0.548(7) |
| O1 | 2*d* | 1 | 1/3 | 2/3 | 0.1967(9) | 1.16(5) |
| O2 | 6*g* | 1 | 0.4668(4) | 0.3167(4) | 0.3151(5) | 1.53(7) |
| O3 | 6*g* | 1 | 0.2215(4) | 0.0777(4) | 0.7614(4) | 1.50(6) |

(c) Atomic parameter of NGS

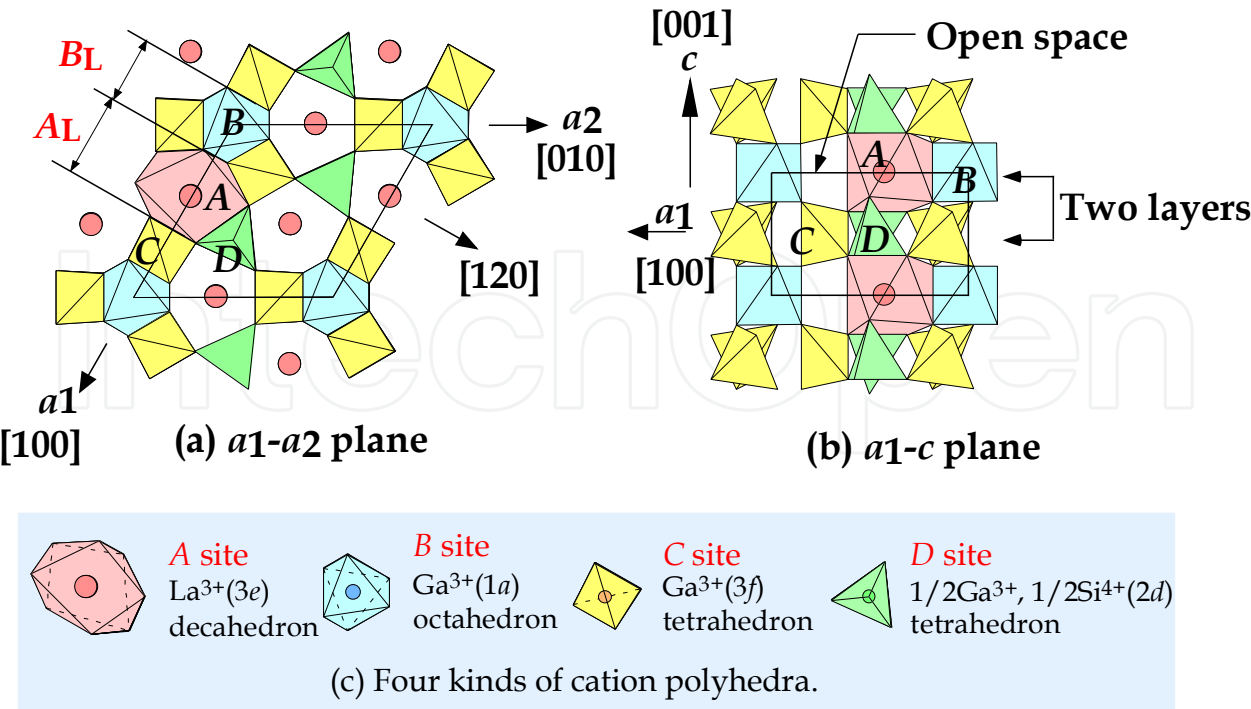| atom | site | occupancy | $x$ | $y$ | $z$ | $B_{eq.}$ (Å$^2$) |
|------|------|-----------|-----|-----|-----|-------------------|
| Nd | 3*e* | 1 | 0.41796(3) | 0 | 0 | 0.660(3) |
| Ga1 | 1*a* | 1 | 0 | 0 | 0 | 0.782(8) |
| Ga2 | 3*f* | 1 | 0.76466(6) | 0 | 1/2 | 0.669(7) |
| Ga3<br>Si | 2*d* | 0.498(3)<br>0.502 | 1/3 | 2/3 | 0.5351(2) | 0.557(8) |
| O1 | 2*d* | 1 | 1/3 | 2/3 | 0.198(1) | 1.33(6) |
| O2 | 6*g* | 1 | 0.4674(4) | 0.3181(4) | 0.3131(7) | 1.63(8) |
| O3 | 6*g* | 1 | 0.2218(4) | 0.0762(4) | 0.7597(5) | 1.50(7) |

Table 3. Atomic paremeters of LGS, PGS and NGS.

Fig. 8. Crystal structure of Langasite. (a) and (b) are viewed from [001] and [120], respectively. (c) is four kinds of cation polyhedra.

The crystal structures among LGS, PGS and NGS differ mostly in shape of each site. In particular, the change of the $A$-site is remarkable. The decahedral $A$-site expands with the increase of ionic radius of rare earth ($R$) that occupies the $A$-site. The $A$-site expands greatly in [100] directions compared to the expansion in [120], which is perpendicular to [100], with the increase of the ionic radius of $R$.

## 4. Piezoelectric properties of langasite

### 4.1 langasite and properites

Langasite shows piezoelectricity but none ferroelectricity, based on crystallographic point group 32 belonging the 4th group in Table 1. This point group is the same with that of quartz showing excellent piezoelectricity. As langasite is none polar piezoelectric crystal, poling treatment is not necessary. However ceramics that is polycrystals show isotropic properties as a whole because each orientation of grains turns to every direction. So, non-polar piezoelectric materials should be used as a single crystal. For a single crystal, the knowledge of the directions of piezoelectricity is very important. As the directions are the same one of polar, they could be derived based on the point group. The Piezoelectric constants of the point group 32 for langasite is as following tensor:

$$\begin{bmatrix} d_{11} & -d_{11} & 0 & d_{14} & 0 & 0 \\ 0 & 0 & 0 & 0 & -d_{14} & -2d_{11} \\ 0 & 0 & 0 & 0 & 0 & 0 \end{bmatrix} \tag{4}$$

Figure 9 shows the stereographic projection of general positions on point group. Figure 9(a) shows [001] direction without polarity because of the same number positions on the

opposite directions of [001] that is same number ◯ and x. [210] direction (Figure 9(c)) also is non-polarity by the same manner. Only [100] direction shows polarity as shown in Figure 9(b). The configurations of a typical crystal with a point group 32 are shown along the stereographic projections, which crystal surfaces are plotted on the stereo projections. The crystal structures along [120] and [100] as shown in Figure 9(d) and (e) show asymmetry, and symmetry, respectively, along left and right directions. Now, Figure 10 shows *Y*-cut of crystal. Here, *X*, *Y*, and *Z* are Cartesian coordination, and hexagonal axis *a* and *c* also are shown.
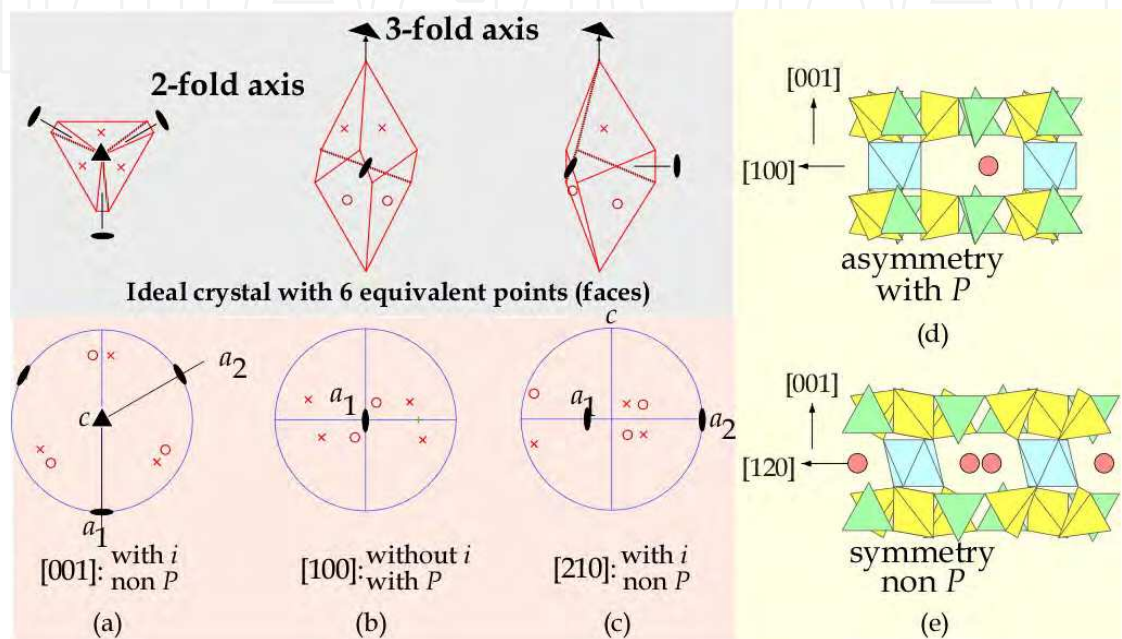


Fig. 9. Determination of piezoelectricity direction based on point group 32. Stereo graphs (a), (b) and (c) with equivalent points are projected from [001], [100], and [210], respectively. X: upper points, o: opposite points. Configurations of a crystal with point group 32 also are drown for supporting the stereo projections. (d) and (e) show the crystal structure along [100] and [120] showing asymmetry and symmetry, respectively. Dipole moment will be appeared in (d).

Figure 11(a) shows equivalent series resistance as a function of vibration modes of resonators on the LGS and quartz single crystals (Shimamura, 1996). The resistance of LGS is one order smaller than that of quartz. So, as if the surface roughness of LGS is large, high frequency oscillation is easy. Moreover, as the equivalent series resistances at high vibration mode as 7th and 9th are small, LGS filter is useful for high frequency wave area filter. Figure 11(b) shows electromechanical coupling factor $k_{12}$ as a function of piezoelectric constant -$d_{11}$ on the langasite group such as LGS. PGS, NGS and so on, comparing quartz single crystal. Figure 12(a) shows electromechanical coupling factor $k^2$ as a function of *TCf* on the piezoelectric materials. The value of langasite is near zero. Figure 12(b) shows temperature dependence of frequency and equivalent series resistance of filter made of Y-cut LGS single crystal (Shimamura, 1996). The temperature dependence of frequency shows a secondary curve with good values of 1-2 ppm/°C. In the range of -20 to 70 °C, the dependence of temperature is good value of 100 to 150 ppm/°C. Table 4 shows the properties comparing some piezoelectric crystals such as

LiTaO$_3$, LGS, quartz, and La$_3$Ga$_{5.5}$Nb$_{0.5}$O$_{14}$ (LGN) (Fukuda et al. 1998). The properties of LGS locate between LiTaO$_3$ and quartz. Electro-mechanical coupling factor $k$ of LGS is 15 to 25 % locating between that of LiTaO$_3$ 43 % and quartz 7 %. The temperature frequency variation of LGS is 100 to 150 ppm/$^o$C locating between that of LiTaO$_3$ 200 to 400 ppm/$^o$C and quartz 50 to 80 ppm/$^o$C. Here, LGN single crystal substituted Nb$^{5+}$ and Ga$^{3+}$ for Si$^{4+}$ has superior properties for piezoelectric properties. Figure 13 shows Pass band characteristic of filter made of Y-cut LGS single crystal (Fukuda, 1995). Y-cut LGS single crystal has a very wide pass band characteristic width of 45 KHz at 3 dB attenuation which is 3-times that of quartz with 15 KHz band width. This means the electromechanical coupling constant $K_{12}$ of LGS is about 3-times larger than that of quartz.
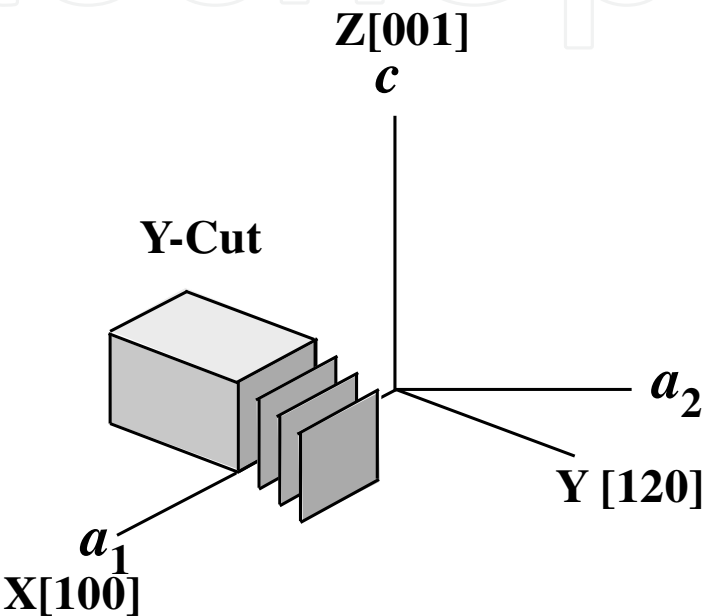


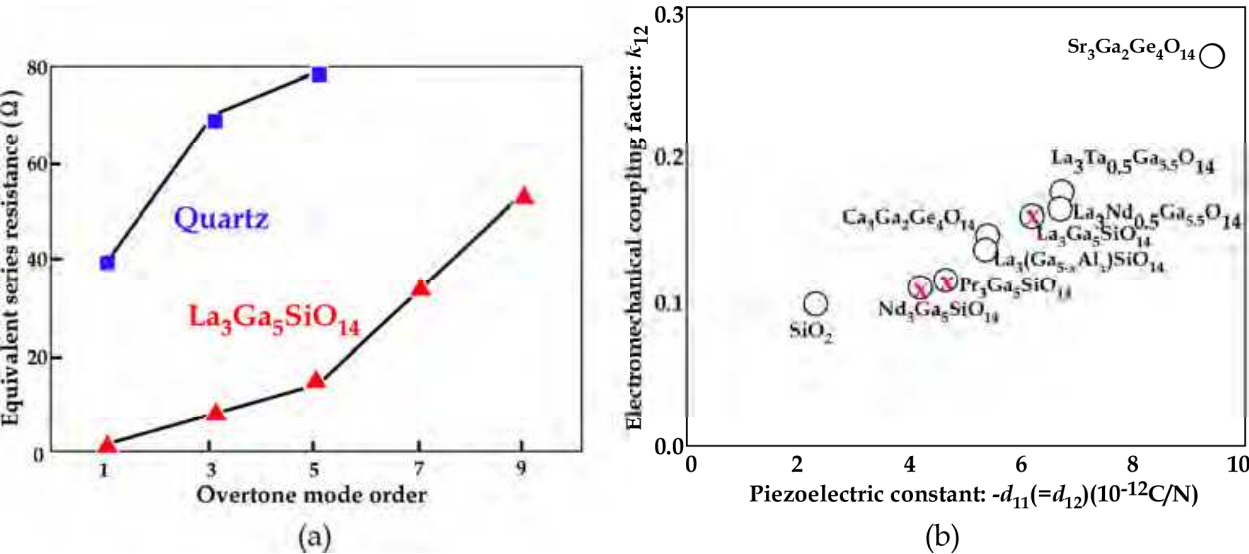Fig. 10. Y-cut for langasite single crystal for piezoelectric measurements.



Fig. 11. (a) Equivalent series resistance of quartz and langasite single crystals as a function of resonator vibration modes. (b) electromechanical coupling factor of langasite series as a function of piezoelectric constant.
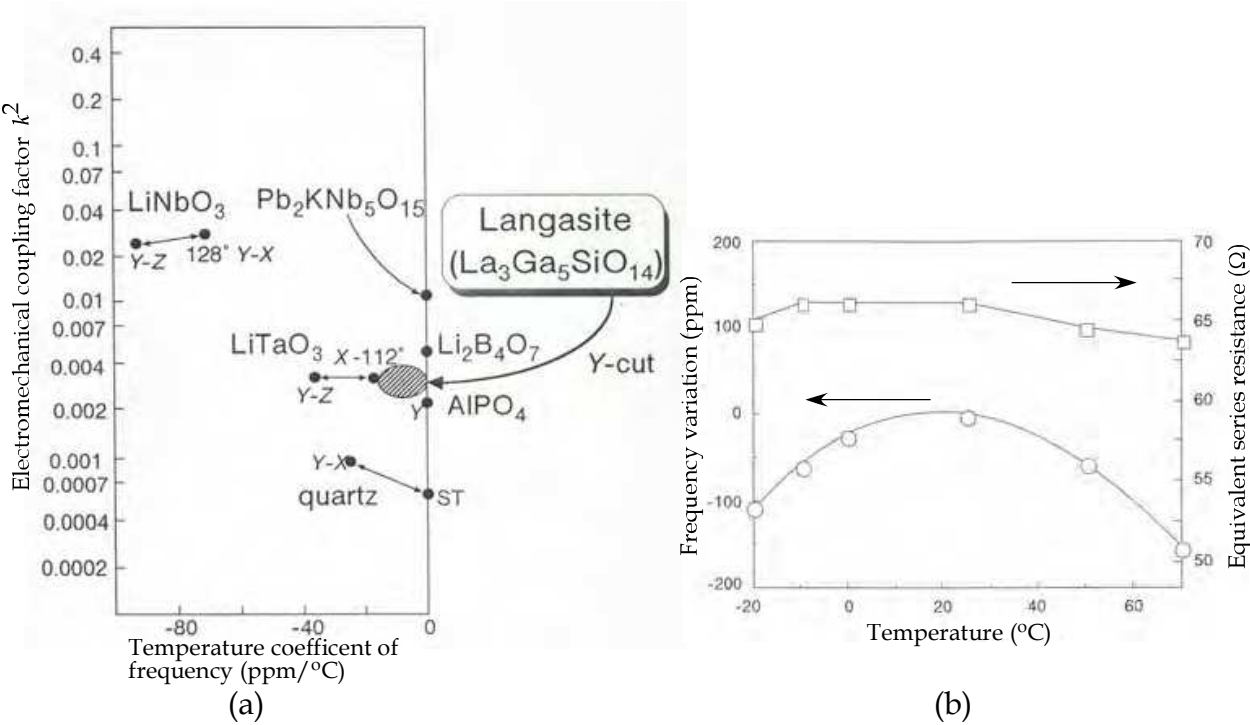
Fig. 12. (a) Electromechanical coupling factor vs. temperature coefficent of frequency of piezeelectric materials. (b) Frequency variation/equivalent series resistance as a function of temperature on the $La_3Ga_5SiO_{14}$ filter.
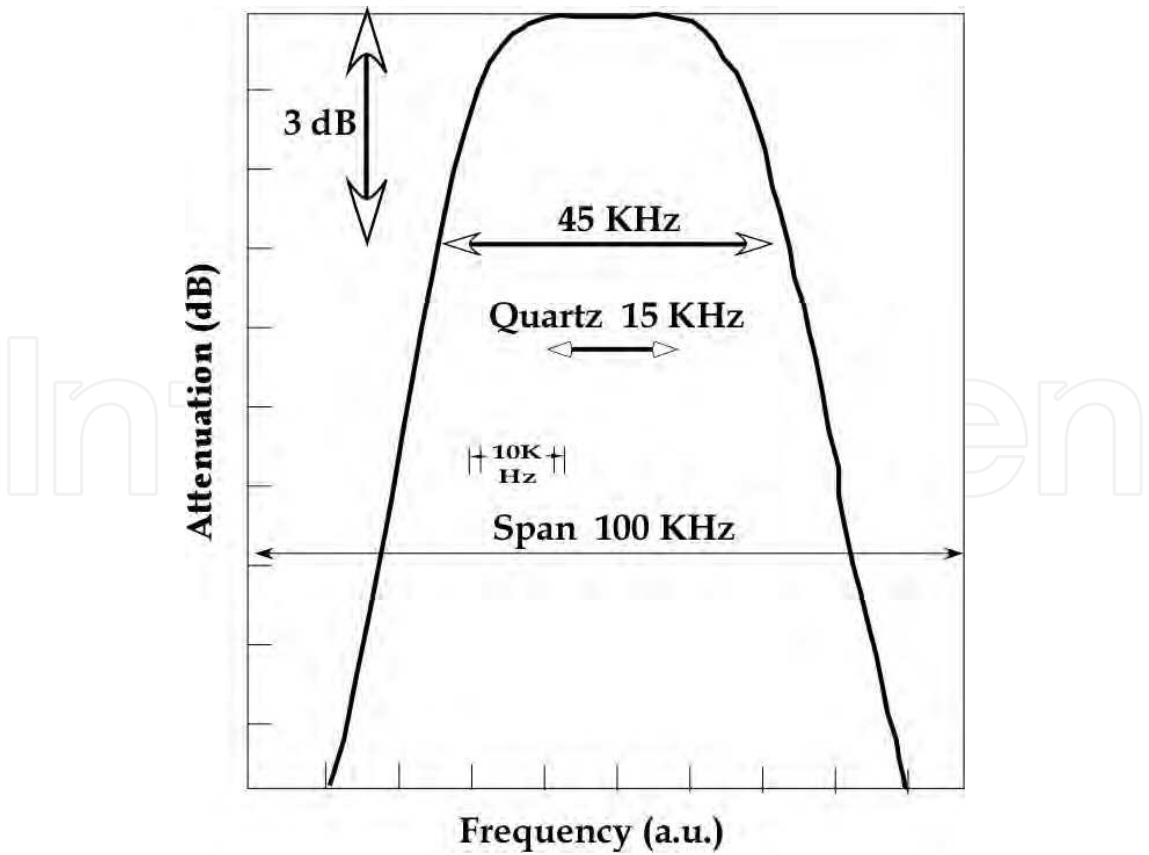


Fig. 13. Filter properties of $La_3Ga_5SiO_{14}$ single crystal.

| | $LiTaO_3$ | $La_3Ga_5SiO_{14}$ | $La_3Ga_{5.5}Nb_{0.5}O_{14}$ | Quartz |
|---|---|---|---|---|
| phase transition | 665°C | none | none | 573°C |
| melting temp. (°C) | 1650 | 1470 | 1470 | —— |
| mohs hardness | 5~6 | 6~7 | 6~7 | 7 |
| electro-mechanical coupling factor $k$ [%] | 43 | 15~25 | ~30 | 7 |
| $Q$ value | 5000 | 30000~40000 | 60000~120000 | 100000~200000 |
| equivalent series resistance [Ω] | —— | 2~5 | 0.7~1.7 | 20~40 |
| frequency variation [ppm] (−20~70°C) | 200~400 | 100~150 | —— | 50~80 |

Table 4. Comparison of properties of each crystal.

## 4.2 Ordered crystal structure and properties

LGS, PGS and NGS having been described here are compositionally disordered crystals. The structural formulae are $[R_3]_A[Ga]_B[Ga_3]_C[GaSi]_DO_{14}$ ($R$ = La, Pr and Nd). Here, as $D$-site is occupied disorderly by Ga and Si, these crystals are disordered. An ordered langasite structural formula such as $Sr_3TaGa_3Si_2O_{14}$ (STGS), $Sr_3TaGa_3Ge_2O_{14}$ (STGG), $Sr_3NbGa_3Si_2O_{14}$ (SNGS), $Ca_3NbGa_3Si_2O_{14}$ (CNGS), and $Ca_3TaGa_3Si_2O_{14}$ (CTGS) are presented and characterized by Mill et al., (1998) and Takeda et al., (2000). The structural formula is $[Sr/Ca_3]_A[Nd/Ta]_B[Ga_3]_C[Ge/Si]_DO_{14}$ : large $A$-decahedron is occupied by Sr or Ca cations, middle size $B$-octahedron by Nd or Ta cations, and $C$- and $D$-tetrahedra by the larger Ga and the smaller Ge or Si cations, respectively. The ordering should be called as "compositional ordering" compared with ordering based on the order-disorder transition.

Table 5 shows characterization of disordered and ordered langasite-type piezoelectric single crystals at room temperature and 500 ᵒC (Zhang, 2009). Though the ordered crystals posess lower piezoelectric coefficients than disordered ones at room temperature, they posess much higher mechanical quality factor and electrical resistivity at elevated temperature of 500 ᵒC. The high mechanical quality factor and the high electrical resistivity has been expected for a high-temperature bulk acoustic wave (BAW) and SAW resonator and ignition pressure sensor, respectively. Density and dielectric constant of ordered cyrstals are lower than those of disordered ones, which contribute to the high acoustic velocity on the high frequency devices. LTGA and LNGA disordered crystals in the Table 5 are substituted Al for Ga on the $La_3R_{0.5}Ga_{5.5-x}Al_xO_{14}$ (L$R$GA$x$, $R$=Ta or Nb), which are contributed to the low raw material cost. Takeda et al. (2005) presented LTG, LTGA0.3 and 0.5 in which $d_{14}$ values are increased 3.68, 4.03 and 4.19 pC/N in the order, and those resistivity increased 2.2 x $10^7$, 4.6 x $10^7$ and 7.1 x $10^8$ Ω•cm in the order at 400 ᵒC as shown in Figure 14 (Takeda et al., 2005). The resistivity of LTGA0.5 increased about 30 times of that of LTG. Also Al-substituted LGS ($La_3Ga_{5-x}Al_xSiO_{14}$: LGAS$x$) are studied for high resistivity at elevated temperature and low cost, which are presented by Kumatoriya et al. (2001), Takeda et al. (2002). The piezoeoectric properties $d_{11}$ and resistivity of LGAS0.9 was improved from 6.075 to 6.188 pC/N and 5.9 x $10^7$ to 7.6 x $10^8$ Ω•cm, respectively. The Al-substitution is effective for high resistivity and also reduce the raw material cost. CTAS in the Table 5 is substituted Al for Ga compleatly which has high resistivity of 2.7x$10^9$ Ω•cm. On the other hand, Fe-

substituted langasite-type crystals are expected for multiferroic materials (C. Lee, et al., 2010).

| Material | Structure | Density (g/cm$^3$) | $\varepsilon_{11}$ | Loss | $K_{12}$ | $s^E_{11}$ (pm$^2$/N) | $d_{11}$ (pC/N) | 500 $^o$C | | |
|---|---|---|---|---|---|---|---|---|---|---|
| | | | | | | | | $Q$ | $\rho$ ($\Omega$ cm) | $RC$ (ms) |
| LGS | Disordered | 5.85 | 18.0 | >0.001 | 0.16 | 8.86 | 6.20 | ··· | 9.0x10$^6$ | 0.02 |
| LTG | Disordered | 6.12 | 19.6 | >0.001 | 0.17 | 9.07 | 7.10 | ··· | 1.5x10$^7$ | 0.03 |
| LNG | Disordered | 5.95 | 20.7 | >0.001 | 0.18 | 9.27 | 7.40 | ··· | 5.0 x10$^7$ | 0.10 |
| LTGA | Disordered | 6.07 | 21.0 | >0.001 | 0.16 | 9.15 | 6.60 | 1000 | 2.2 x10$^7$ | 0.05 |
| LNGA | Disordered | 5.90 | 19.5 | >0.001 | 0.16 | 9.90 | 6.90 | 1000 | 1.1 x10$^8$ | 0.22 |
| SNGS | Ordered | 4.65 | 12.4 | <0.001 | 0.17 | 8.80 | 5.40 | 7500 | 6.3 x10$^7$ | 0.08 |
| STGS | Ordered | 5.12 | 11.8 | <0.001 | 0.16 | 8.69 | 4.90 | 11000 | 3.7 x10$^8$ | 0.42 |
| CNGS | Ordered | 4.15 | 17.5 | <0.001 | 0.11 | 8.75 | 4.00 | 8000 | 6.9 x10$^7$ | 0.11 |
| CTGS | Ordered | 4.63 | 16.5 | <0.001 | 0.11 | 8.95 | 4.00 | 19000 | 1.7 x10$^9$ | 2.36 |
| CTAS | Ordered | 4.04 | 13.0 | <0.001 | 0.14 | 8.51 | 4.30 | 20000 | 2.7 x10$^9$ | 3.25 |

Table 5. Characterization of disordered and ordered langasite-type piezoelectric single crystals at room temperature and 500 $^o$C. LTG:La$_3$Ta$_{0.5}$Ga$_{5.5}$O$_{14}$; LNG:La$_3$Nb$_5$GaO$_{14}$; LTGA: La$_3$Ta$_{0.5}$Ga$_{5.3}$Al$_{0.2}$O$_{14}$; LNGA: La$_3$Nb$_{0.5}$Ga$_{5.3}$Al$_{0.2}$O$_{14}$;SNGS: Sr$_3$NbGa$_3$Si$_2$O$_{14}$; STGS: Sr$_3$TaGa$_3$Si$_2$O$_{14}$; CNGS: Ca$_3$NbGa$_3$Si$_2$O$_{14}$; CTGS: Ca$_3$TaGa$_3$Si$_2$O$_{14}$;CTAS: Ca$_3$TaAl$_3$Si$_2$O$_{14}$.
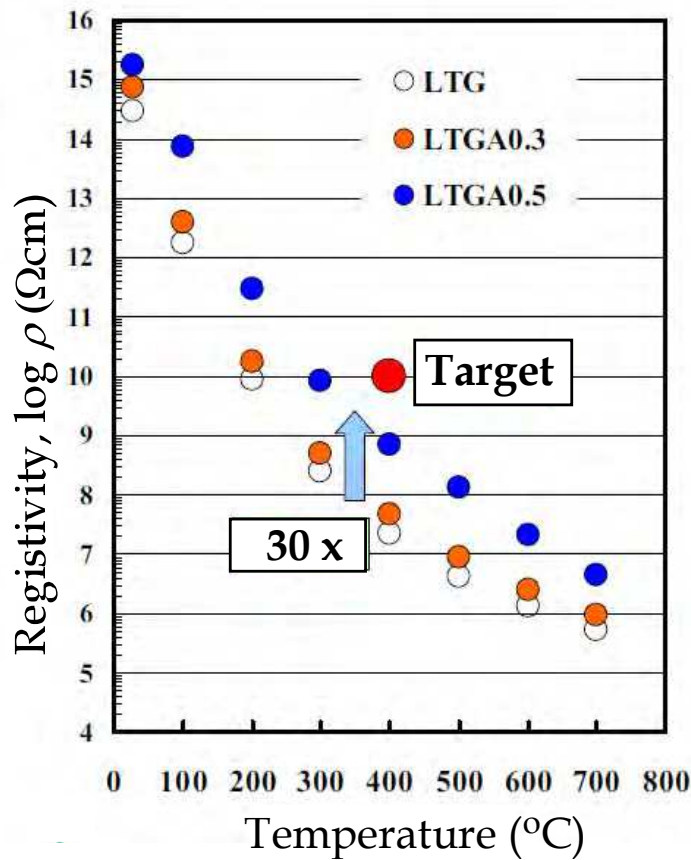


Fig. 14. Resistivity of LTG, LTGA0.3 and 0.5 at elevated temperature. Al-substituted LTG 0.5 was improved about 30 times at 400 $^o$C. More high resistivity is expected.

## 5. Mechanism of piezoelectricity of langasite based on the crystal structure

In this section, mechanism of piezoelectricity of langasite will be presented based on the crystal structure. Fukuda et al. (1995) and Sato et al. (1998) presented an excellent relationship between the piezoelectric properties of LGS, PGS and NGS, and the lattice parameters and the ionic radius of $R$-ion in $A$-decahedron as shown in Figure 15(a) and (b), respectively. Now, we will consider the reason why LGS has the best piezoelectric properties among LGS, PGS and NGS. The volumes of $A$-site increase depending on the ionic size, and the lattice parameter of $a$-axis elongates by 0.100 Å larger than that 0.023 Å of $c$-axis based on the crystal structure as described section 3. Deformation of $A$-site along [100] direction might bring the piezoelectricity. The direction is just direction generating the piezoelectricity as shown in Figure 9 described in the Section 4. So, we will consider the deformation of $A$-site based on the crystal structure obtained. Figure 16 shows the deformation of $A$-decahedron. This decahedron is a twisted Thomson cube with 8 coordination numbers composed of three kinds of oxygen ions: O1, O2 and O3 as shown in Table 3 in Section 3. Here, important oxygen ions for the deformation are named by I, II and III as shown in Figure 16. The I anion is O3, and the II and III anions are equivalent of O2 by 3-fold axis. Here, O1 on the top oxygen of $D$-tetrahedron just located on the 3-fold axis. These I, II and III anions are shifted toward arrow direction in Nd, Pr and La order based on the crystal structure obtained. For the III anion, coordinate $x$ increased, and $y$ also increased. On the contrary, for the II anion, coordinate $x$ decreased and $y$ also decreased. As a result, the $A$-site deforms anisotropically as expanding to [100] and shrinking to [120] direction. Though other sites also deform a little, the explanations will be elsewhere because it is not so important for piezoelectric properties in this crystal structure. This $A$-site deformation compared with $B$-site: $A_L/B_L$ as shown in Figure 17(a) has relationships with piezoelectric constant $d_{11}$ and electromechanical coupling factor $k_{12}$ as shown in Figure 17(b). Here, $A_L$ and $B_L$ are lengths of $A$-site and $B$-site along [100], respectively. Three components compounds: LGS, PGS and NGS show just linear relationship with $d_{11}$ and $k_{12}$.
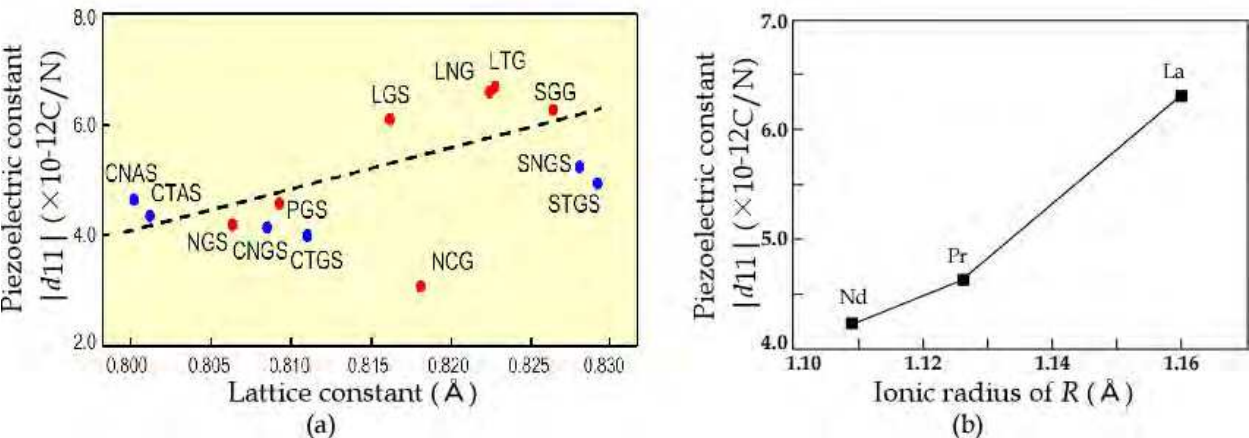


Fig. 15. (a) Piezoelectric constant $d_{11}$ as a function of lattice constant for Langasite series crystals. (b) $d_{11}$ of LGS, RGS and NGS as a function of ionic radius.

Iwataki et al. (2001) also shows relationship between $A_{L1}/A_{L2}$ and piezoelectric modulus $|d_{11}|$ as shown in Figure 18. Here, $A_{L1}$ is same length with $A_L$ as shown in Fig.17, and $A_{L2}$ is length along [120] of $A$-polyhedron. As seen from Figure 18(b), the ratio $A_{L1}/A_{L2}$ increases

with the ionic radius of $R$ and the piezoelectric modulus also increases. The ratio shows distortion of $A$-polyhedron, and large distortion brings high $d_{11}$. LGS with large La ion brings larger $d_{11}$ more than PGS and NGS with Pr and Nd, respectively.
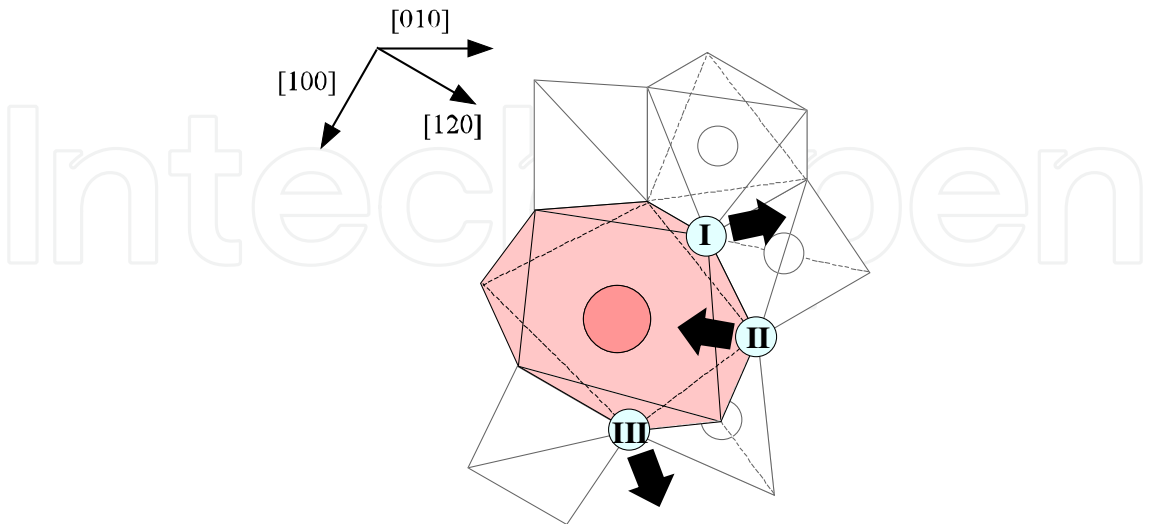


Fig. 16. Deformation of $A$-decahedron. I:O3, II and III:O2. When $A$-site was occupied by large ion such as La, the $A$-site will be deformed to arrow direction of oxygen ions anisotropically.
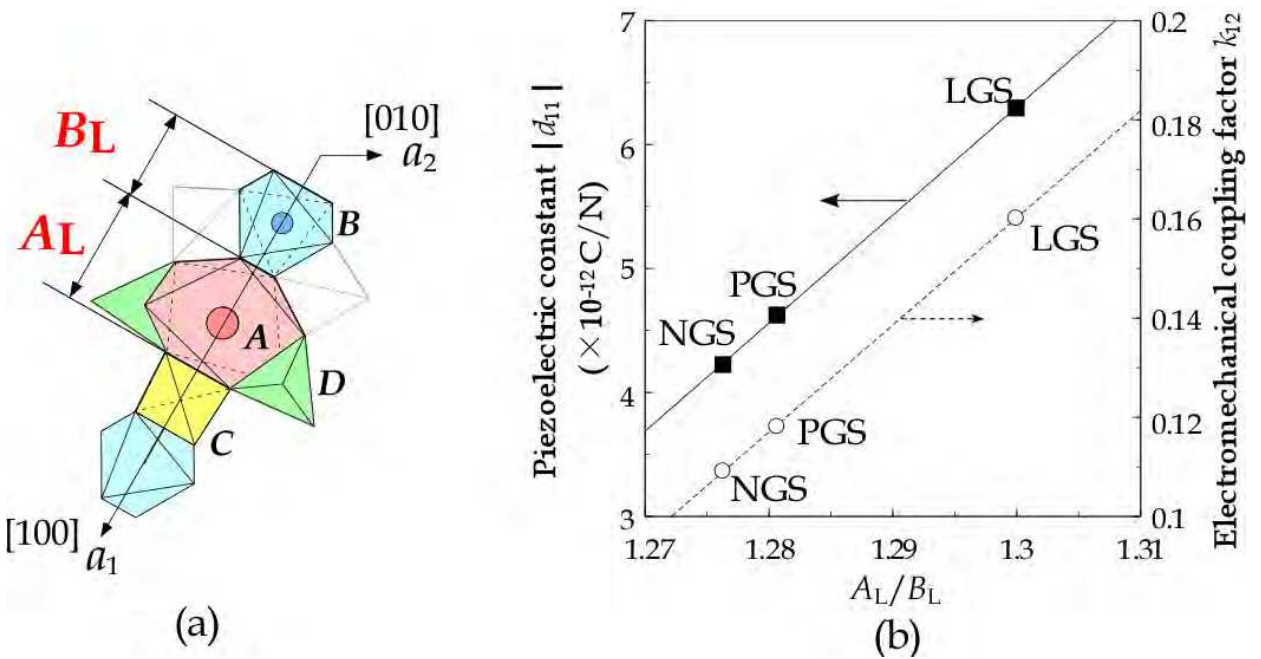


Fig. 17. (b) Piezoelectric constant $d_{11}$/electromechanical coupling factor $k_{12}$ of LGS, PGS and NGS as a function of $A_L/B_L$ which is shown in (a).

We will consider a mechanism for piezoelectricity based on the information obtained before. The direction for piezoelectricity is [100] direction based on point group 32 as shown in Figure 9 described in Section 4. Along the [100] direction, there are two cation polyhedra: $A$-decahedron and $B$-octahedron, and open-space located among the polyhedra, which play an important role for piezoelectricity as sown in Figure 19. $B$-ions in octahedron locate on the
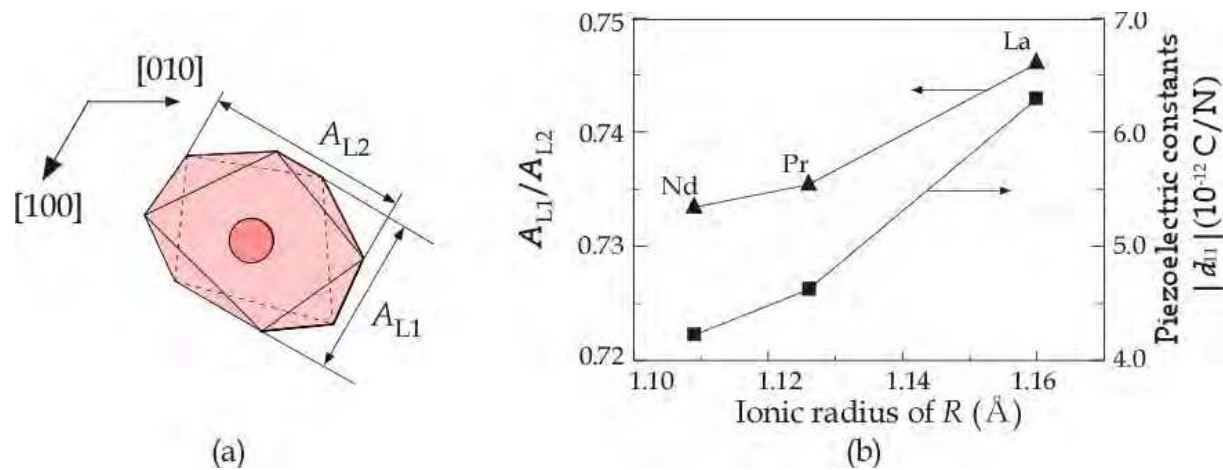
Fig. 18. (a) Size $A_{L1}$ and $A_{L2}$ of $A$-polyhedron along [100] and [120], respectively. (b) The ratio $A_{L1}/A_{L2}$ and piezoelectric modulus $|d_{11}|$ as a function of ionic radius of $R$.

origin of unit cell, and $A$-ion locates in the decahedron contacted with $B$1-octahedron and open-space.
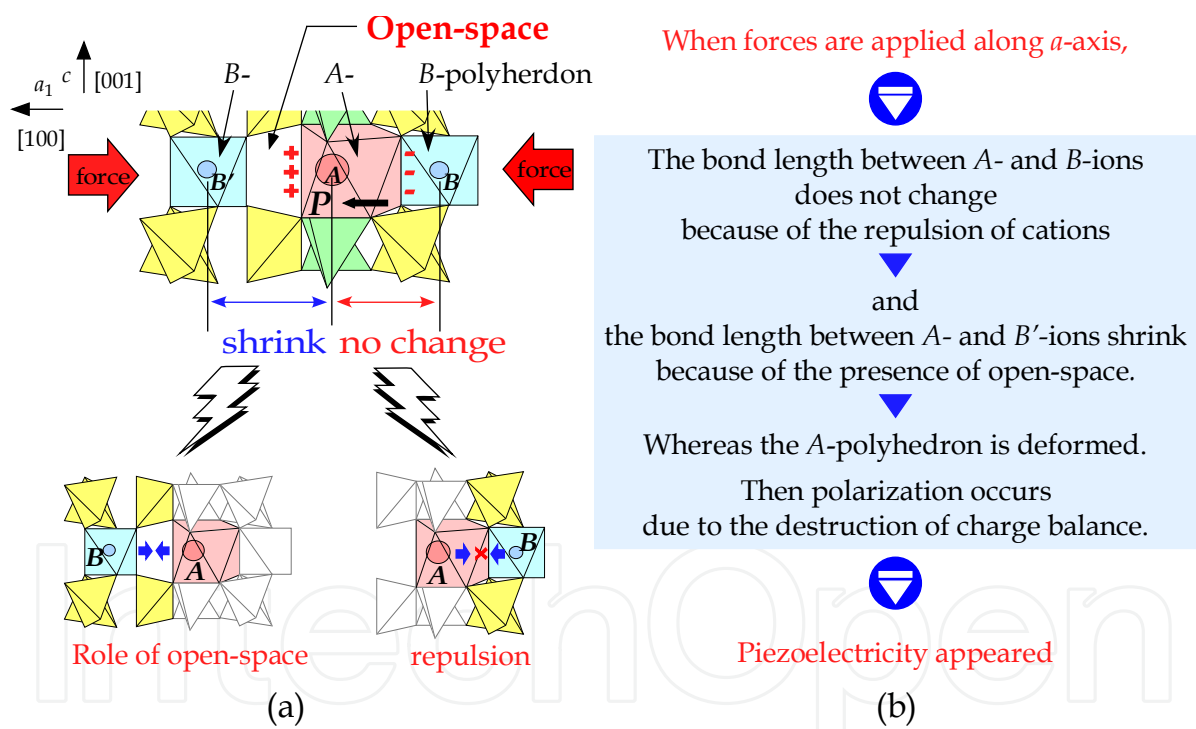


Fig. 19. Mechanism of piezoelectricity presented imaginary based on role of open-space in the crystal structure.

With an induced pressure, though all polyhedra are compressed, distances between cations show different movements. The distance between $A$ and $B$ shows no change, and that between $A$ and $B'$ shows shrinkage. This phenomenon could be explained by the existence of open-space, that is, no change in the distance between $A$ and $B$ should be generated by the repulsion between the cation charges and by the role of shock absorption of the open-space. The shrinkage between $A$ and $B'$ is generated by the shock absorption of the open-space. As a result, the position of $A$-cation is shifted from the center of the decahedron, so, it

brings the piezoelectricity that the centers of mass of positive charges and negative charges are in different positions.

## 6. Crystal structure and piezoelectricity under pressure

In this section, the mechanism of the piezoelectricity presented imaginary in section 5 will be confirmed under applied pressure. Pressures applied to the single crystals using a diamond anvil cell (DAC) as shown in Figure 20 were calibrated by the ruby fluorescence technique. The DAC was putted on the four-circle diffractmeter. The unit cell parameters were refined by using the $2\theta$-$\omega$ step scan technique.

Table 6 shows crystallographic data of LGS and NGS including the lattice parameters measured at various pressures. The pressure dependence of lattice parameters ($a_1$ and $c$) and unit cell volume are plotted in Figure 21. Both of lattice parameters along $a_1$- and $c$-directions shrunk linearly with an increase of applied pressure. Noteworthy is that the $a_1$-axis is preferentially shrunk direction compared to the $c$-axis. This indicates that the compression of langasite crystals occurs preferentially in the $a_1$-$a_2$ plane.
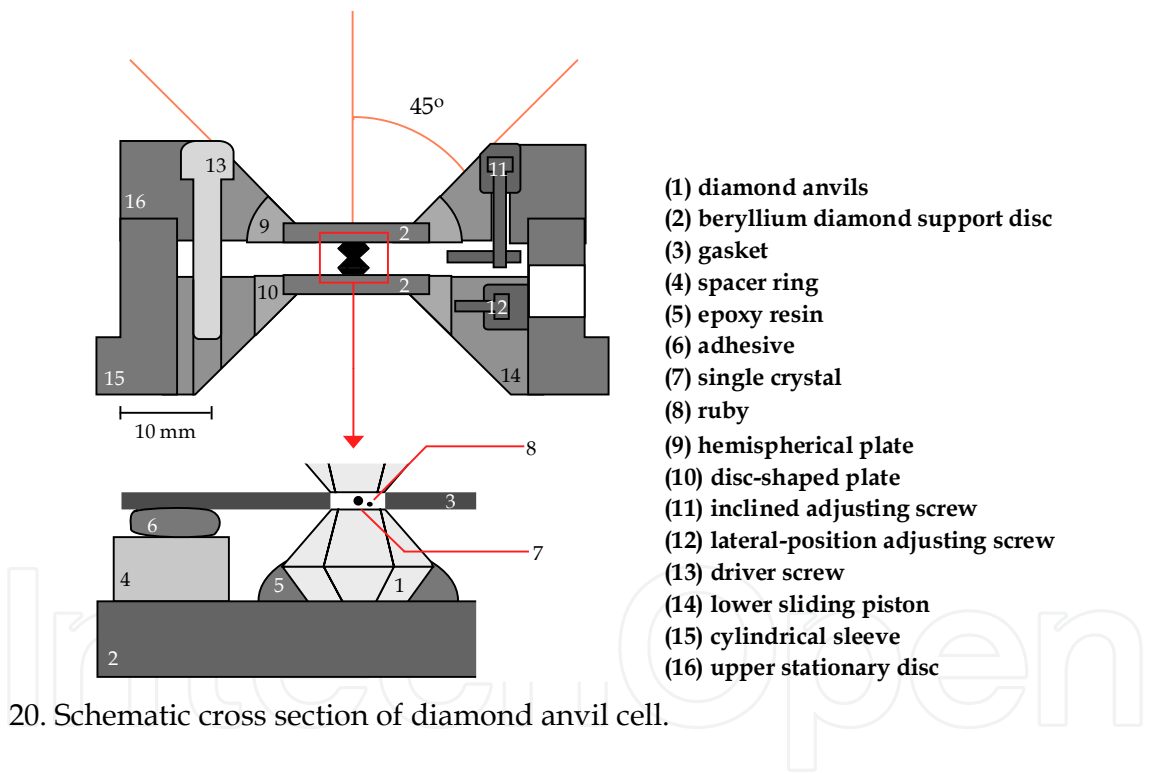


**(1) diamond anvils**
**(2) beryllium diamond support disc**
**(3) gasket**
**(4) spacer ring**
**(5) epoxy resin**
**(6) adhesive**
**(7) single crystal**
**(8) ruby**
**(9) hemispherical plate**
**(10) disc-shaped plate**
**(11) inclined adjusting screw**
**(12) lateral-position adjusting screw**
**(13) driver screw**
**(14) lower sliding piston**
**(15) cylindrical sleeve**
**(16) upper stationary disc**

Fig. 20. Schematic cross section of diamond anvil cell.

| | LGS | | | NGS | | |
|---|---|---|---|---|---|---|
| Pressure (GPa) | Atm. | 3.3 | 6.1 | Atm. | 3.5 | 6.8 |
| Lattice parameter $a$ (Å) | 8.1674(4) | 8.103(1) | 8.046(3) | 8.0674(5) | 7.999(1) | 7.926(1) |
| $c$ (Å) | 5.0964(8) | 5.070(1) | 5.052(1) | 5.0636(9) | 5.041(1) | 5.011(1) |
| Unit cell volume (Å$^3$) | 294.41(5) | 288.3(1) | 283.2(1) | 285.40(5) | 279.4(1) | 272.6(1) |
| Calculated density $D_x$ (g/cm$^3$) | 5.7384 | 5.860 | 5.965 | 6.013 | 6.143 | 6.295 |
| Linear absorption coefficient $m$ (cm$^{-1}$) | 228.496 | 233.339 | 237.505 | 258.608 | 264.210 | 270.751 |
| $R$ | 3.45 | 4.70 | 6.01 | 3.17 | 5.88 | 4.48 |
| $wR$ | 3.60 | 5.59 | 7.03 | 3.30 | 6.78 | 5.17 |

Table 6. Crystallographic data of LGS and NGS under pressure.

(a) Atomic parameter of LGS at atmospheric pressure

| atom | site | occupancy | $x$ | $y$ | $z$ | $Beq.$ ($\text{Å}^2$) |
|------|------|-----------|-----|-----|-----|------------------------|
| La | $3e$ | 1 | 0.41862(3) | 0 | 0 | 0.632(3) |
| Ga1 | $1a$ | 1 | 0 | 0 | 0 | 0.849(8) |
| Ga2 | $3f$ | 1 | 0.76514(6) | 0 | 1/2 | 0.665(7) |
| Ga3 | $2d$ | 0.5 | 1/3 | 2/3 | 0.5324(2) | 0.553(7) |
| Si | | 0.5 | | | | |
| O1 | $2d$ | 1 | 1/3 | 2/3 | 0.196(1) | 1.14(5) |
| O2 | $6g$ | 1 | 0.4655(5) | 0.3114(5) | 0.3165(7) | 1.43(7) |
| O3 | $6g$ | 1 | 0.2218(5) | 0.0816(5) | 0.7639(6) | 1.57(8) |

(b) Atomic parameter of LGS at 3.3 GPa

| atom | site | occupancy | $x$ | $y$ | $z$ | $Beq.$ ($\text{Å}^2$) |
|------|------|-----------|-----|-----|-----|------------------------|
| La | $3e$ | 1 | 0.4212(3) | 0 | 0 | 1.00(4) |
| Ga1 | $1a$ | 1 | 0 | 0 | 0 | 1.4(1) |
| Ga2 | $3f$ | 1 | 0.7671(5) | 0 | 1/2 | 1.08(7) |
| Ga3 | $2d$ | 0.5 | 1/3 | 2/3 | 0.531(2) | 1.1(1) |
| Si | | 0.5 | | | | |
| O1 | $2d$ | 1 | 1/3 | 2/3 | 0.199(7) | 1.4(5) |
| O2 | $6g$ | 1 | 0.456(4) | 0.306(3) | 0.306(5) | 2.2(4) |
| O3 | $6g$ | 1 | 0.224(3) | 0.084(3) | 0.765(4) | 1.6(3) |

(c) Atomic parameter of LGS at 6.1 GPa

| atom | site | occupancy | $x$ | $y$ | $z$ | $Beq.$ ($\text{Å}^2$) |
|------|------|-----------|-----|-----|-----|------------------------|
| La | $3e$ | 1 | 0.4216(4) | 0 | 0 | 0.94(6) |
| Ga1 | $1a$ | 1 | 0 | 0 | 0 | 1.4(2) |
| Ga2 | $3f$ | 1 | 0.7675(8) | 0 | 1/2 | 0.96(10) |
| Ga3 | $2d$ | 0.5 | 1/3 | 2/3 | 0.531(2) | 0.8(2) |
| Si | | 0.5 | | | | |
| O1 | $2d$ | 1 | 1/3 | 2/3 | 0.205(8) | 1.0(7) |
| O2 | $6g$ | 1 | 0.459(5) | 0.308(4) | 0.312(6) | 2.2(5) |
| O3 | $6g$ | 1 | 0.217(5) | 0.080(5) | 0.757(5) | 2.2(6) |

(d) Atomic parameter of NGS at atmospheric pressure

| atom | site | occupancy | $x$ | $y$ | $z$ | $Beq.$ ($\text{Å}^2$) |
|------|------|-----------|-----|-----|-----|------------------------|
| Nd | $3e$ | 1 | 0.41796(3) | 0 | 0 | 0.658(3) |
| Ga1 | $1a$ | 1 | 0 | 0 | 0 | 0.776(7) |
| Ga2 | $3f$ | 1 | 0.76460(6) | 0 | 1/2 | 0.667(6) |
| Ga3 | $2d$ | 0.5 | 1/3 | 2/3 | 0.5352(2) | 0.559(7) |
| Si | | 0.5 | | | | |
| O1 | $2d$ | 1 | 1/3 | 2/3 | 0.196(1) | 1.31(6) |
| O2 | $6g$ | 1 | 0.4673(5) | 0.3174(5) | 0.3104(7) | 1.60(7) |
| O3 | $6g$ | 1 | 0.2234(5) | 0.0771(5) | 0.7607(5) | 1.46(7) |

(e) Atomic parameter of NGS at 3.5 GPa

| atom | site | occupancy | $x$ | $y$ | $z$ | $Beq.$ ($\text{Å}^2$) |
|------|------|-----------|-----|-----|-----|------------------------|
| Nd | $3e$ | 1 | 0.4193(4) | 0 | 0 | 1.02(6) |
| Ga1 | $1a$ | 1 | 0 | 0 | 0 | 1.1(2) |
| Ga2 | $3f$ | 1 | 0.7667(9) | 0 | 1/2 | 1.12(10) |
| Ga3 | $2d$ | 0.5 | 1/3 | 2/3 | 0.535(2) | 0.8(2) |
| Si | | 0.5 | | | | |
| O1 | $2d$ | 1 | 1/3 | 2/3 | 0.189(9) | 2.2(10) |
| O2 | $6g$ | 1 | 0.469(5) | 0.322(5) | 0.316(5) | 2.1(6) |
| O3 | $6g$ | 1 | 0.227(5) | 0.076(5) | 0.770(5) | 2.5(6) |

(f) Atomic parameter of NGS at 6.8 GPa

| atom | site | occupancy | $x$ | $y$ | $z$ | $Beq.$ ($\text{Å}^2$) |
|------|------|-----------|-----|-----|-----|------------------------|
| Nd | $3e$ | 1 | 0.4227(3) | 0 | 0 | 0.79(5) |
| Ga1 | $1a$ | 1 | 0 | 0 | 0 | 1.2(1) |
| Ga2 | $3f$ | 1 | 0.7688(7) | 0 | 1/2 | 0.90(8) |
| Ga3 | $2d$ | 0.5 | 1/3 | 2/3 | 0.534(1) | 1.0(1) |
| Si | | 0.5 | | | | |
| O1 | $2d$ | 1 | 1/3 | 2/3 | 0.181(8) | 2.3(9) |
| O2 | $6g$ | 1 | 0.467(6) | 0.319(4) | 0.312(5) | 2.6(5) |
| O3 | $6g$ | 1 | 0.224(5) | 0.075(4) | 0.768(5) | 3.1(6) |

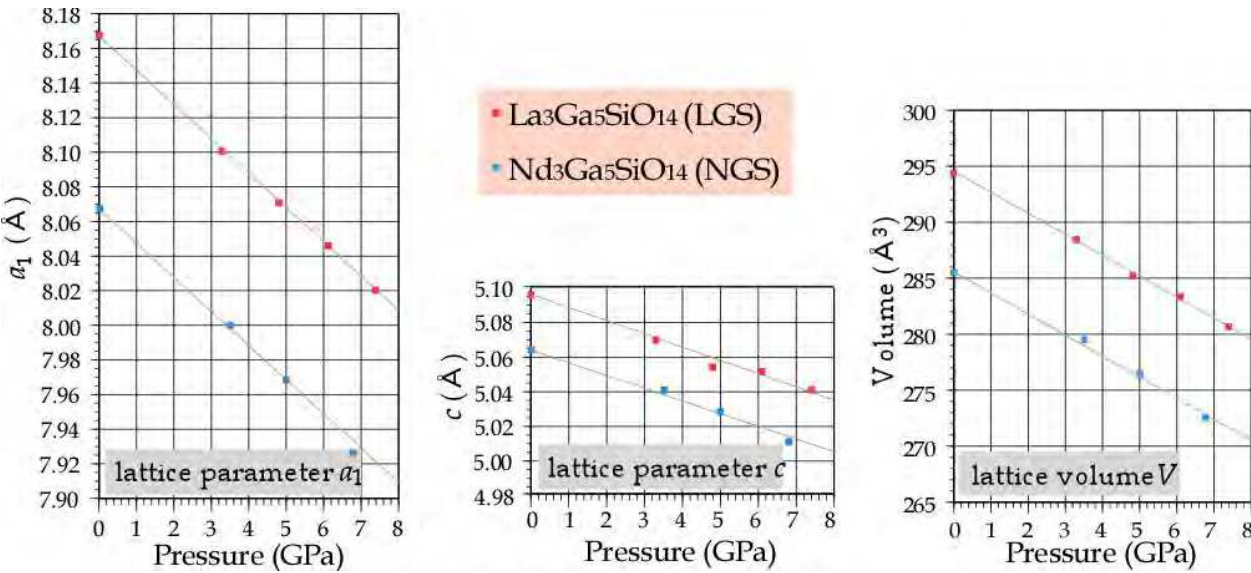Table 7. Atomic parameter of LGS (a) to (c) and NGS (d) to (f) under the pressure.

Fig. 21. Lattice parameters and volume of LGS and NGS as a function of pressure.

Table 7 shows atomic parameters of LGS and NGS under pressure. The site occupancies of Ga and Si ions on the $D$-site are fixed to 0.5 according to the data as shown in Table 3. The temperature coefficients are calculated from anisotropic temperature coefficients obtained. Bond lengths and volumes of this structure are calculated from these data. Table 8 compares the variation of $A_L$, $B_L$ and $S_L$, presented in Figure 22, along [100] direction between atmospheric pressure, around 3 and 6 GPa. Lattice parameter $a_1$ equals the sum of $A_L+B_L+S_L$. Therefore, we can consider that preferential shrinkage observed along $a_1$-axis is also divided into three kinds of length. As seen in Table 8, the change in $S_L$ is much larger than the other length of $A_L$ and $B_L$, indicating a larger contribution of shrinkage of an open-space. The open-space forms corner shares with $A$- and $B$-polyhedra. In contrast, $A$- and $B$-polyhedra make shared edges with each other. When the pressure induced in the [100] direction, it can be speculated that the corner-shared open-space is easily distorted compared with the edge-shared $A$- and $B$-polyhedra.

| | LGS | | | NGS | | |
|---|---|---|---|---|---|---|
| | Pressure (GPa) | | | Pressure (GPa) | | |
| (Å) | Atm. | 3.3 | 6.1 | Atm. | 3.5 | 6.8 |
| $A_L$ | 3.516 | 3.541 | 3.536 | 3.411 | 3.324 | 3.413 |
| $B_L$ | 2.956 | 2.949 | 2.848 | 2.982 | 3.024 | 2.869 |
| $S_L$ | 1.694 | 1.612 | 1.661 | 1.674 | 1.652 | 1.644 |
| $A_L/B_L$ | 1.19 | 1.20 | 1.24 | 1.14 | 1.10 | 1.19 |

Table 8. $A$- and $B$-polyhedra size $A_L$ and $B_L$, and open-space size $S_L$ along $a$-axis and $A_L/B_L$ for LGS and NGS. Atm.: atmosphere pressure.

| $M_L$, $N_L$, $O_L$, Dipole moment ($M_L$-$O_L$) and $a_1$ (Å) | LGS | | | NGS | | |
|---|---|---|---|---|---|---|
| | Pressure (GPa) | | | Pressure (GPa) | | |
| | Atm. | 3.3 | 6.1 | Atm. | 3.5 | 6.8 |
| $M_L$ | 3.419 | 3.413 | 3.392 | 3.372 | 3.354 | 3.350 |
| $N_L$ | 4.748 | 4.690 | 4.654 | 4.696 | 4.645 | 4.576 |
| $O_L$ | 3.271 | 3.249 | 3.215 | 3.229 | 3.203 | 3.172 |
| $M_L$- $O_L$ | 0.148 | 0.164 | 0.177 | 0.143 | 0.151 | 0.178 |
| $a_1$ | 8.167 | 8.103 | 8.046 | 8.067 | 7.999 | 7.926 |

Table 9. Atomic distances ($M_L$, $N_L$), center position X-$B$ ion distance ($O_L$), dipole moment ($M_L$ - $O_L$) and lattice constant of $a_1$ of LGS and NGS along [100] direction under the pressure. Atm.: atmosphere pressure.
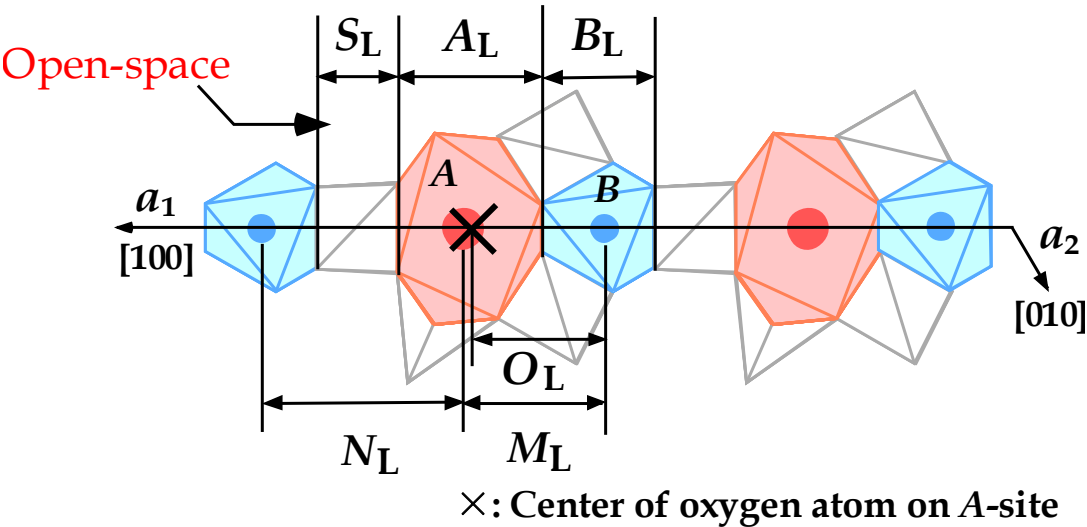


Fig. 22. Sizes of $A$-, $B$-site and open space $S$, and atomic distances of $M_L$, $N_L$ and $O_L$ between atoms. Position X is the center of oxygen atoms on $A$-polyhedron.

Piezoelectricity is originated from polarization caused by the destruction of charge balance depending on the displacement of ions when pressure is induced. The piezoelectricity of langasite is known to be generated in the [100] direction. From the rule of symmetrical operation, langasite should have polarization in $A$- and $C$-polyhedra in contrast with no polarization in $B$- and $D$-polyhedra. We have already stated the mechanism of piezoelectricity imaginary on Langasite as shown in Figure 19 in section 5. In this section, evidence of the mechanism is clarified based on crystal structure analysis under the pressure. And also, the reason of La-langasite having larger piezoelectricity than Nd-langasite is clarified. With an induced pressure, distance $M_L$ between $A$ and $B$ cations as shown in Figure 22 and Table 9 is not changed around 3.4 Å, and distances of $N_L$ ($A$ ion-[open-space]-$B$ ion) in LGS and NGS are shrunk from 4.75 to 4.65, and 4.70 to 4.58 Å, respectively. On the other hand, $A$-polyhedron is distorted to [$\bar{1}$00] direction. The distortion is clarified by shortage of distance $O_L$ between center position X on $A$-polyhedron and $B$-ion as shown in Figure 22 and 23. The $O_L$ lengths of LGS and NGS are shortened from 3.27 to 3.21 Å, and 3.23 to 3.17 Å, respectively. As a result, a dipole moment $P$ appeared according to moving the centers of mass of positive and negative charges to produce piezoelectricity.
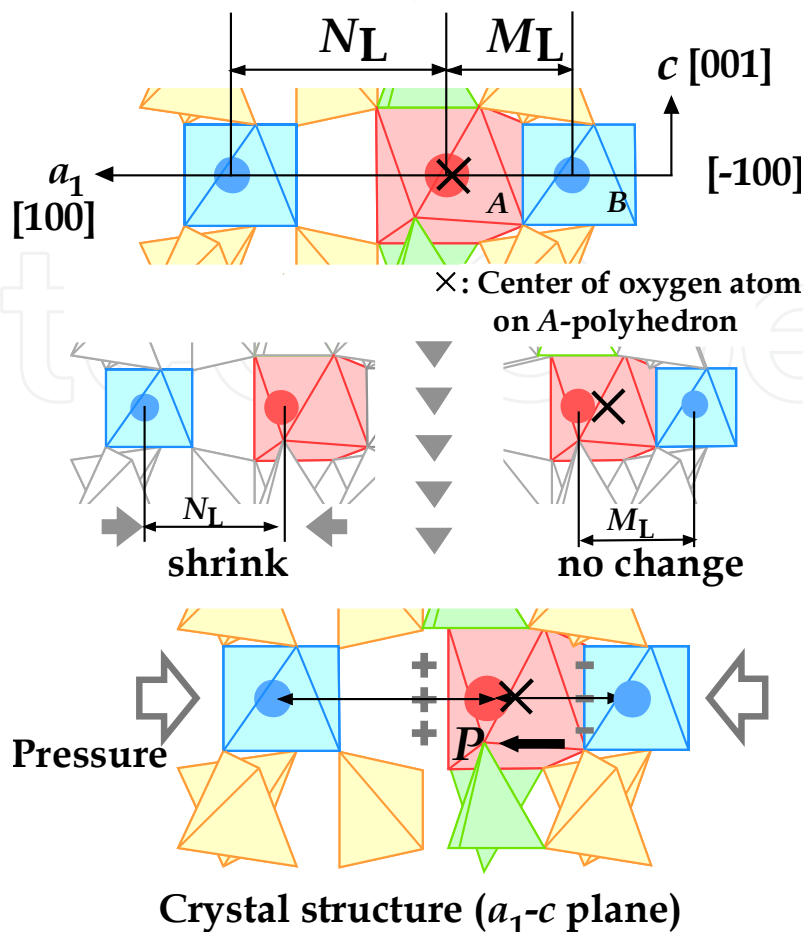
Fig. 23. Origin of piezoelectricity on Langasite projected from [120]. Position X is the center of oxygen atoms on $A$-polyhedron. Under pressure, $ML$ does not chang and $NL$ shrinks $A$-ion.

Here, differences ($M_L$-$O_L$) between center positions X and $A$-ion positions on the LGS and NGS calculated based on crystal structure are equivalent to polarization as shown in Table 9, and Figure 24. The values of LGS and NGS as a function of pressure are increased from 0.147 to 0.177 Å (at 6.1 GPa) and 0.143 to 0.178 Å (at 6.8 GPa), respectively. The value increases with pressure. So, the mechanism of piezoelectricity on the langasite structure series is clarified as follows: though the $A$-polyhedron is deformed to [$\bar{1}00$] with applied force, $A$-ion stay on same position by repulsion force from $B$-ion under the existence of open-space which has no atoms in the center and is working as damper. The difference between $A$-cation and center position X should make a net dipole moment $P$ along $a$-axis. Dipole moment should be enhanced if the distance between the charge centers of cations and anions becomes large. Therefore, the enhancement of piezoelectric properties is related with the shrinkage of open-space in langasite crystal structure, and it is clear that the increase of polarization is caused by the induced pressure in [1 0 0] direction of langasite structure.

The reason of La-langasite having larger piezoelectricity than Nd-langasite is clarified by the difference of the $M_L$-$O_L$ (dipole moments $P$). As shown in Figure 24, the dipole moments $P$ for LGS are larger than that for NGS.
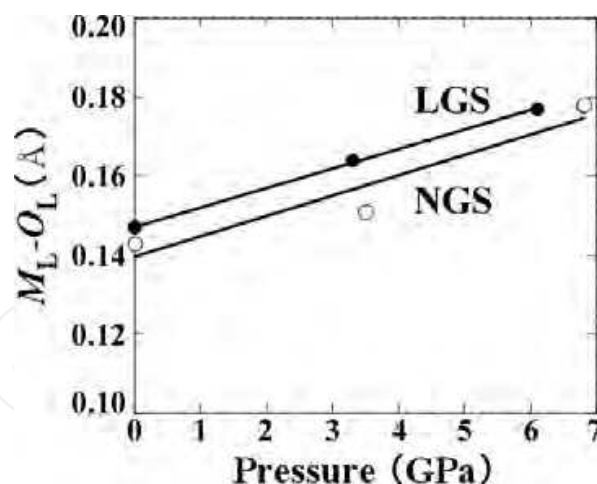
Fig. 24. The difference $M_L$-$O_L$ (dipole moment P) for LGS and NGS as a function of pressure.

## 7. New piezoelectric materials with framework structure

Langasite is a kind of materials with framework structure without inversion symmetry $i$. quartz and BeO are also framework structure which is formed mainly by a covalent bond such as $SiO_4$, $AlO_4$, $ZnO_4$. Especially, silicates including langasite make many framework structures by connection of $SiO_4$ tetrahedra as cyclo-, ino-, phyllo-, and tecto-silicates. These framework structures are noticed recently for applications on many kinds of properties such as zeolite for optical properties by absorption of special compounds.

Here, we will present a candidate for piezoelectric materials. Nepheline ($KNa_3Al_4Si_4O_{16}$) is one of the alumino-silicates with framework as shown in Figure 25(a). The crystal structure has hexagonal ring framework without $i$ based on the space group $P6_3$ (No. 173), the point group 6. When stress will be added to the ring, the ring will deform and cations located in tetrahedra and near the center of ring will shift. If the center of cations and anions will become different, piezoelectricity will occur.

Recently, Hosono (2010) presented that $Ca_{12}Al_{14}O_{32}$ ($C_{12}A_7$) clinker compound with big cages including $O^{2-}$ in a $[Ca_{24}Al_{28}O_{64}]^{4+}$ framework shows specific properties such as electride, transparent electride, transparent p-type conducting oxides, transparent semiconductor, super conductor, etc. The crystal structure has 12 cages of 4.4 Å in diameter in a unit cell of 12 Å cube, and 2 cages of 12 cages include oxygen ion ($O^{2-}$) as shown in Figure 25(b). As this $O^{2-}$ is bonding weakly with the framework, this ion could be removed or exchanged with other anions easily. Transparent metal oxide ($C_{12}A_7$:H⁻) transformed to electro conductor by photon induced phase transition, $C_{12}A_7$ compound including much active oxygen O⁻ atoms (Hayashi et al., 2002), and $C_{12}A_7$: e⁻ electride stable in room temperature and air-condition (Matsuishi et al., 2003) are presented by Hosono group.

This $C_{12}A_7$ crystal grown by Cockayne & Lent (1979) is expected for SAW, because of the high SAW velocity and reasonable bulk electromechanical coupling by Whatmore (to be published). Two space groups are reported such as $I\bar{4}3d$ by Cockayne & Lent (1979) and $I\bar{4}2m$ by Kurashige et al. (2006). The point groups are $\bar{4}3m$ and $\bar{4}2m$, respectively. Both point groups without $i$ show piezoelectricity and the latter shows additional rotatory power. Moreover, additional atoms group in the cages of the frame structure are expected to be designed for SAW suitable properties.
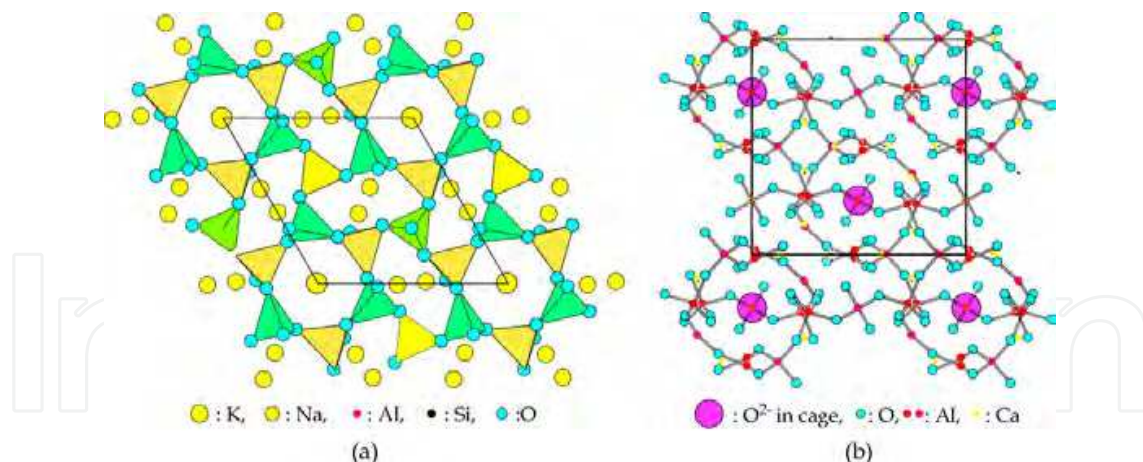
Fig. 25. (a) Nepheline structure as an example of alumino-silicates with framework. (b) Crystal structure of aluminate calcium $C_{12}A_7$. New-type superior properties such as super-conductor were designed from this structure.

## 8. Conclusion

Origin of piezoelectricity on Langasite has been explained based on the crystal structure, and clarified by crystal structure analysis under high pressure. In the introduction, the principle of piezoelectricity and present condition required such as Pb-free piezoelectricity are stated. Next, crystal growth of langasite, crystal structure analysis and piezoelectric properties of langasite are stated, and mechanism of piezoelectricity are presented based on the crystal structure and properties. And the mechanism is confirmed by crystal structure analysis under high pressure. Finally, a search of new piezoelectric materials are proposed on the direction of framework compound such as nepheline, and introduced the $C_{12}A_7$ compounds with framework also for piezoelectricity.

## 9. Acknowledgment

## 10. References

Araki, N., (2004). "Crystallographic Study for the piezoelectric mechanism of langasite under high pressure, electric field & high & low temperature." *Master-thesis of Nagoya Institute of Technology*.

Araki, N., Ohsato, H., Kakimoto, K., Kuribayashi, T., Kudoh, Y., & Morikoshi, H., (2007). "Origin of Piezoelectricity for Langasite $A_3Ga_5SiO_{12}$ (A = La & Nd) under high Pressure" *J. Eur. Ceram. Soc.*, 27, pp. 4099-4102.

Belokoneva, E. L., Simonov, M. A., Butashin, A. V., Mill, B. V., & Belov, N. V., (1980). "Crystal structure of calcium gallogermanate $Ca_3Ga_2Ge_4O_{14}$ = $Ca_3Ge[(Ga_2Ge)Ge_2O_{14}]$ and its analog $Ba_3Fe_2Ge_4O_{14}$ = $Ba_3Fe[(FeGe_2)Ge_2O_{14}]$" *Sov. Phys. Dokl.*, 25, pp. 954-957.

Bussen, W., & Eitel, A., (1936). "Die Struktur des Pentacalciumtrialuminats" *Z. Kryst.*, 95, pp. 175-188. (Germany).

Cockayne, B., & Leat, B., (1979). "SINGLE CRYSTAL GROWTH OF 12 CaO 7 $Al_2O_3$" *J. Crystal Growth*, 46(2) pp. 467-473.

European Commission - Environment - Waste – WEEE. Date of access: 2nd, November, 2011, [web1]http://ec.europa.eu/environment/waste/weee/index_en.htm [web2]http://ec.europa.eu/environment/waste/weee/pdf/hazardous_substances_report.pdf

Fukuda, T., Shimamura, K., Kohno, T., Takeda, H., & Sato, M., (1995). "New Piezoelectric Crystal "Langasite" *J. Jap. Asso. Crystal Growth*, 22(5), 358-363. (Japanese)

Fukuda, T., Takeda, H., Shimamura, K., Kawanaka, H., Kumatoriya, M., Murakami, S., Sato, J., Sato, M., (1998). "Growth of New Langasite Single Crystals for Piezoelectric Applications" *Proceedings of the Eleventh IEEE International Symposium*, ISBN:0-7803-4959-8, Montreux, Switzerland, August 1998.

Guo, Y., Kakimoto, K., & Ohsato, H., (2004). "Phase transitional behaviour and piezoelectric properties of $(Na_{0.5}K_{0.5})NbO_3$-$LiNbO_3$ ceramics" *App. Phys. Lett.*, 18, pp. 4121-4123.

Hayashi, K., Hirano, M., Matsuishi, S., & Hosono, H., (2002). "Microporous Crystal $12CaO•7Al_2O_3$ Encaging Abundant O-Radicals" *J. Am. Chem. Soc.*, 124, pp. 738-739.

Hosono, H., (2010). Chap.10, in Handbook of Transparent Conductors, Edited by Ginley, D., Hosono, H., & Paine, D., Springer.

Hosono, H., Hayashi, K., Kamiya, T., Atou, T., & Susaki:, T., (2011). "New functionalities in abundant element oxides: ubiquitous element strategy" *Sci. Technol. Adv. Mater.*, 12, PP. 034303 (22pp).

Hosono, Y., & Yamashita, Y., (2004). "High-Efficiency Piezoelectric Single Crystal", *Toshiba Review*, 59(10), pp. 39-42.

Iwataki, T., (2002). "Study for the relationship between crystal structure and piezoelectric properties of langasite-type piezoelectric crystals" *Master-thesis of Nagoya Institute of Technology*. (Japanese)

Iwataki, T., Ohsato, H., Tanaka, K., Morikoshi, H., Sato, J., & Kawasaki, K., (2001). "Mechanism of the piezoelectricity of langasite based on the crystal structures" *J. Eur. Ceram. Soc.*, 21, pp. 1409-1412.

Kakimoto, K., Masuda I., & Ohsato, H., (2004). "Ferroelectricity and Solid-Solution Structure of $KNbO_3$ Ceramics Doped with La and Fe" *Key Eng. Mater.*, 269, pp. 7-10.

Kaminskii, A. A., Mill, B. V., Khodzhabagyan, G. G., Konstantinova, A. F., Okorochkov, A. I., & Silvestrova, M., (1983). "Investigation of trigonal $(La_{1-x}Nd_x)_3Ga_5SiO_{14}$ crystals. I. Growth and optical Properties" *Physica Status Solidi (a)*, 80(1), pp. 387–398.

Katsuro, H., Matsuishi, S., Kamiya, T., Hirano, M., & Hosono, H., (2002). "Light-induced conversion of an insulating refractory oxide into a persistent electronic conductor" *Nature*, 419, pp. 462-465.

Kazuhisa, K., Toda, Y., Matsuishi, S., Hayashi, K., Hirano, M., & Hosono, H., (2006). "Czochralski Growth of $12CaO•7Al_2O_3$ Crystals" *Cryst. Growth Design*, 6, pp. 1602-1605.

Kumatoriya, M., Sato, H., Nakanishi, J., Fujii, T., Kadota M., & Sakabe, Y., (2001). "Crystal growth and electromechanical properties of Al substituted langasite $(La_3Ga_{5-x}Al_xSiO_{14})$" *J. Cryst. Growth*, 229, pp. 289-293.

Lee, C., Kan, E., Xiang, H., & Whangbo, M. H., (2010). "Theoretical Investigation of the Magnetic Structure and Ferroelectric Polarization of the Multiferroic Langasite $Ba_3NbFe_3Si_2O_{14}$" *Chem. Mater.*, 22(18), pp. 5290-5295.

Matsuishi, S., Toda, Y., Miyakawa, M., Hayashi, K., Kamiya, T., Hirano, M., Tanaka, I., & Hosono, H. (2003). "High Density Electron Anions in a Nano-porous Single Crystal: $[Ca_{24}Al_{28}O_{64}]^{4+}(4e\text{-})$" *Science*, 301, pp. 626-629.

Mill, B. V., Belokoneva, E. L., & Fukuda, T., (1998). "New compounds with a $Ca_3Ga_2Ge_4O_{14}$-Type Structure: $A_3XY_3Z_2O_{14}$ (A = Ca, Sr, Ba, Pb; X = Sb, Nb, Ta; Y = Ga, Al, Fe, In; Z = Si, Ge)" *Russian J. Inorg. Chem.* 43, pp. 1168-1175. Translated from *Zh. Neorganicheskoi Khimii*, 43, pp. 1270-1277.

Mill, B. V., Buntashin, A. V., Khodzhabagyan, G. G., Belokoneba, E. L., & Belov, N. V. (1982). "Modified rare-earth gallates with a $Ca_3Ga_2Ge_4O_{14}$ structure" *Dokl. Akad. Nauk SSSR*, 264, pp. 1385-1389.

Mill, B. V.; Butashin, A. V.; Khodzhabagyan, G. G.; Belokoneva, E. L.; Belov, N. V., (1982). "Modified rare-earth gallates with a $Ca_3Ga_2Ge_4O_{14}$ structure" *Sov. Phys. Dokl.*, 27, pp. 434-437.

Saito, Y., Takao, H., Tani, T., Nonoyama, T., Takatori, K., Homma, T., Nagaya, T., & Nakamura, M., (2004). "Lead-free piezoceramics" *Nature*, 432, pp. 84-87.

Sasaki, S., (1982). "A Fortran program for the least-squares refinement of crystal structure" *XL Report, ESS, State Univ. of New York*, pp.1-17.

Sato, J., Takeda, H., Morikoshi, H., Shimamura, K., Rudolph, P. & Fukuda, T. (1998). "Czochralski growth of $RE_3Ga_5SiO_{14}$ (RE=La, Pr, Nd) single crystals for the analysis of the influence of rare earth substitution on piezoelectricity" *J. Crystal Growth*, 191, pp. 746-753.

Shimamura, K., Kato, T., Sato, J., & Fukuda, T., (1999). "Crystal Growth and Characterization of New Langasite-type Compounds for Piezoelecteic Applications" *Proceedings of The 9th US-Japan on Dielectric and Piezoelectric Ceramics*, held November 2-5, Rizzan Sea Park Hotel, Tancha Bay, Okinawa, Japan.

Shimamura, K., Takeda, H., Kohno, T., & Fukuda, T., (1996). "Growth and characterization of lanthanum gallium silicate $La_3Ga_5SiO_{14}$ single crystals for piezoelectric applications" *J. Crystal Growth*, 163, pp. 388-392.

Takeda, H., Izukawa, S., Shimizu, H., Nishida, T., Okamura, S., & Shiosaki, T.,(2005)."Growth, Structure and Piezoelectric Properties of $Ln_3Ga_5SiO_{14}$ (Ln= La, Nd) Single Crystals"Trans. *Mater. Res. Soc. Jpn.* 30, pp.63-66.

Takeda H., & Tsurumi, T., (2011). "Crystal Growth of High Temperature Piezoelectric Crystals from Quasi-Congruent Melt", *Bulletin of the Ceramic Society of Japan*, 46(8), pp. 657-661.

Takeda, H., (1998). "A Study of the Growth, Structure and Properties of $A_3BC_3D_2O_{14}$-type Complex Oxide Crystals" *Ph. D. Thesis, Tohoku University*.

Takeda, H., Kumatoriya, M., & Shiosaki, T., (2002). "Structure and Piezoelectric Properties of Al-substituted Langasite ($La_3Ga_{5-x}Al_xSiO_{14}$) Crystals" *Key Eng.*, 216, pp. 43-46.

Takeda, H., Sato, J., Kato, T., Kawasaki, K., Morikoshi, H., Shimamura, K., & Fukuda, T., (2000). "Symthesis and characterization of $Sr_3TaGa_3Si_2O_{14}$ single crystals" *Mater. Res. Bull.*, 35, pp.245-252.

Whatmore, R. W., (1980). "New Polar Materials: Their Application to SAW and Other Devices" *J. Crystal Growth*, 48, pp. 530-547.

Zhang, S., Zheng, Y., Kong, H., Xin, J., Frantz E., & Shrout, T. R., (2009). "Characterization of high temperature piezoelectric crystals with an ordered langasite structure" *J. Appl. Phys.*, 105, pp. 114107-1-6.

**Materials Science and Technology**

Edited by Prof. Sabar Hutagalung

ISBN 978-953-51-0193-2

Hard cover, 324 pages

**Publisher** InTech

**Published online** 07, March, 2012

**Published in print edition** March, 2012

Materials are important to mankind because of the benefits that can be derived from the manipulation of their properties, for example electrical conductivity, dielectric constant, magnetization, optical transmittance, strength and toughness. Materials science is a broad field and can be considered to be an interdisciplinary area. Included within it are the studies of the structure and properties of any material, the creation of new types of materials, and the manipulation of a material's properties to suit the needs of a specific application. The contributors of the chapters in this book have various areas of expertise. therefore this book is interdisciplinary and is written for readers with backgrounds in physical science. The book consists of fourteen chapters that have been divided into four sections. Section one includes five chapters on advanced materials and processing. Section two includes two chapters on bio-materials which deal with the preparation and modification of new types of bio-materials. Section three consists of three chapters on nanomaterials, specifically the study of carbon nanotubes, nano-machining, and nanoparticles. Section four includes four chapters on optical materials.

**How to reference**

In order to correctly reference this scholarly work, feel free to copy and paste the following:

Hitoshi Ohsato (2012). Origin of Piezoelectricity on Langasite, Materials Science and Technology, Prof. Sabar Hutagalung (Ed.), ISBN: 978-953-51-0193-2, InTech, Available from:

http://www.intechopen.com/books/materials-science-and-technology/origin-of-piezoelectricity-on-langasite

**INTECH**

open science | open minds